



Contents lists available at [SciVerse ScienceDirect](http://SciVerse.ScienceDirect.com)

Acta Biomaterialia

journal homepage: www.elsevier.com/locate/actabiomat



The dependence of DNA supercoiling on solution electrostatics

David Argudo, Prashant K. Purohit*

Department of Mechanical Engineering and Applied Mechanics, University of Pennsylvania, Philadelphia, PA 19104, USA

ARTICLE INFO

Article history:
Received 4 October 2011
Received in revised form 20 January 2012
Accepted 26 January 2012
Available online xxx

Keywords:

DNA plectonemes
Biological material
Electrostatics
Multivalent counterions
Thermal fluctuations

ABSTRACT

We develop an elastic–isotropic rod model for twisted DNA in the plectonemic regime. We account for DNA elasticity, electrostatic interactions and entropic effects due to thermal fluctuations. We apply our model to single-molecule experiments on a DNA molecule attached to a substrate at one end, while subjected to a tensile force and twisted by a given number of turns at the other end. The free energy of the DNA molecule is minimized subject to the imposed end rotations. We compute values of the torsional stress, radius, helical angle and key features of the rotation–extension curves. We also include in our model the end loop energetic contributions and obtain estimates for the jumps in the external torque and extension of the DNA molecule seen in experiments. We find that, while the general trends seen in experiments are captured simply by rod mechanics, the details can be accounted for only with the proper choice of electrostatic and entropic interactions. We perform calculations with different ionic concentrations and show that our model yields excellent fits to mechanical data from a large number of experiments. Our methods also allow us to consider scenarios where we have multiple plectonemes or a series of loops forming in the DNA instead of plectonemes. For a given choice of electrostatic and entropic interactions, we find there is a range of forces in which the two regimes can coexist due to thermal motion.

© 2012 Acta Materialia Inc. Published by Elsevier Ltd. All rights reserved.

1. Introduction

The mechanical and electrostatic properties of DNA directly affect various cellular processes, such as replication, transcription, compaction and protein–DNA binding. This is the motivation behind this study of DNA supercoils, which are also known as plectonemes. Plectonemes in DNA molecules are manipulated by several molecular machines during key processes, such as transcription and DNA repair [1]. In several scenarios, the action of these molecular machines or enzymes on DNA has been found to depend on the mechanical stress present in the molecules [2,3]. Consequently, DNA supercoiling remains a subject of study for theorists and experimentalists alike.

Experimentally, DNA supercoiling has been investigated using several biochemical and biophysical methods, including single-molecule experimental techniques, where individual DNA molecules can be stretched and twisted under physiologically relevant conditions [4–8]. In these experiments, it is possible to apply a force and/or moment parallel to the filament axis of a DNA molecule, and to measure the elastic response in terms of elongation and angle of twisting about the filament axis. In rotation–extension experiments, the vertical extension of the DNA filament and the external moment are recorded as a function of the number of turns.

It is a well-known feature of the experimental curves that there is a regime, corresponding to the formation of plectonemes, where there is almost a linear relationship between the DNA extension and the applied number of turns. Also, as shown in the recent experiments of Forth et al. [4], Lipfert et al. [5] and Mosconi et al. [6], the external moment is approximately constant in the plectonemic regime.

Plectonemes have been studied theoretically as elastic rods by many authors [9–14]. In order to interpret single-molecule experiments, Purohit [15,16] accounts for the effects of thermal fluctuations as well as electrostatics in plectonemes and straight portions of DNA, and shows that many features seen in the recent experiments of Forth et al. [4] can be qualitatively reproduced using an elastic rod model. Furthermore, as seen in Fig. 5 in Purohit [16], his theoretical results for the slope of the linear region in vertical extension of the DNA vs. number of turns of the bead are around twice the value of those found in experiments by Forth et al. [4]. One of the goals of this paper is to address this problem and get more quantitative agreement with single-molecule experiments. Our approach follows those of van der Heijden et al. [14] and Clauvelin et al. [17,18], who use a variational formulation to solve for the geometry of the plectoneme. The analysis in van der Heijden et al. [14] considers only the elastic energy of the filament, but Clauvelin et al. [17,18] and other authors [19] consider electrostatic interactions together with the elasticity, and are able to reproduce some of the features of the rotation–extension experiments. In agreement

* Corresponding author. Tel.: +215 898 3870; fax: +215 573 6334.
E-mail address: purohit@seas.upenn.edu (P.K. Purohit).

with Purohit [16], Clauvelin et al. [18] reach the conclusion that electrostatics plays a minor role compared to the elasticity of the DNA in these experiments. Contrary to this conclusion, recent single-molecule experiments and molecular simulations have shown that the results of the rotation–extension experiments depend strongly on the salt concentration of the solution [20,21]. For this reason, we carefully consider electrostatics in this paper and present an analytical model that captures the behavior of DNA in rotation–extension experiments and simulations for a variety of DNA lengths, applied loads and salt concentrations. We also apply our model to a novel set of DNA experiments with a mixture of monovalent and multivalent salts, and show that we can predict the results of these experiments.

Other key variables that are affected by the salt concentration are the discontinuities in extension and torque during the supercoiling transition [20]. These discontinuities have been studied recently by Forth et al. [4] and Daniels et al. [22]. Purohit's models [15,16] capture these discontinuities or jumps qualitatively, but he does not comment on the salt dependence of the jumps. We use our model to provide estimates for the number of turns at which the DNA makes a transition from a straight to a supercoiled configuration, and for the jump in the extension and moment as a function of DNA length and salt concentration. Furthermore, we contemplate the possibility of the formation of multiple plectonemes and other forms of DNA compaction (loops and plectonemes coexistence) due to energetic reasons.

2. General description of the model

We proceed with a model of the plectonemic region of the DNA molecule based on the framework of Clauvelin et al. [18], but we account for thermal fluctuation effects, confinement entropy and an end loop model. The DNA in the experiments is modeled as a Kirchhoff inextensible elastic rod of length $2l$ (with $-l \leq s \leq l$, where s is the arc length along the centerline of the rod). The Kirchhoff theory of rods models the centerline as a curve in space $\mathbf{r}(s)$ endowed with mechanical properties which are assumed to be suitable averages over the cross-section of the rod [23,24]. The configuration of an inextensible, unshereable rod is defined by $\mathbf{r}(s)$ and an associated right-handed orthonormal director frame $\mathbf{d}_i(s)$, $i = 1, 2, 3$. For convenience, the vector $\mathbf{d}_3 = \mathbf{r}'(s)$ is taken to be tangential to the rod. The kinematics of the frame are encapsulated in the director frame equations $\mathbf{d}'_i = \mathbf{u} \times \mathbf{d}_i$, where the components of $\mathbf{u} = u_i \mathbf{d}_i$ are measures of the strain, u_3 describes the physical twist, and u_1 and u_2 are associated with bending such that the square of curvature is given by $\kappa^2 = u_1^2 + u_2^2$. We assume a linear constitutive relation between the stresses and the strains, so that the moment $\mathbf{m} = K_b u_1 \mathbf{d}_1 + K_b u_2 \mathbf{d}_2 + K_t u_3 \mathbf{d}_3$, where K_b is the bending modulus and K_t is the twisting modulus. The rod is made up of three regions (see Fig. 1):

- In the linear regions the tails are, on average, aligned with the vertical axis. The tails are not completely straight and the centerline follows a writhing path due to thermal fluctuations in the DNA molecule. An analysis of fluctuating polymers

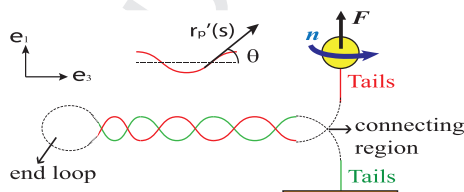


Fig. 1. Sketch representing single-molecule experiments, where a DNA molecule is fixed at one end while the other end is subjected to a pulling force F and twisted by a given number of turns n .

subjected to tension and twist in the straight regime has been carried out in detail by Moroz and Nelson [25,26], where expressions for the twist and writhe have been provided. In our model we will use their expressions.

- In the plectonemic region the position vector $\mathbf{r}_p(s)$ and the tangent vector $\mathbf{r}'_p(s)$ describe the superhelix. Note that each helix is itself a piece of double-stranded DNA molecule. So, in the literature, DNA plectonemic geometrical variables (angle and radius) are often referred to as supercoiling or superhelical, to distinguish them from the intrinsic helical nature of the base pair structure. Due to the symmetry of the problem, it is convenient to introduce cylindrical coordinates (r, ψ, z) for the position vector:

$$\mathbf{r}_p(s) = \chi r \mathbf{e}_r + z \mathbf{e}_3 \quad (1)$$

where \mathbf{e}_3 is the axis of the helix that wraps around the cylinder and $\mathbf{e}_r = \cos\psi \mathbf{e}_1 + \sin\psi \mathbf{e}_2$. The tangent to the position vector is:

$$\mathbf{r}'_p(s) = \sin\theta \theta \mathbf{e}_\psi + \cos\theta \mathbf{e}_3 \quad (2)$$

$$\psi' = \chi \frac{\sin\theta}{r}, \quad z' = \cos\theta, \quad 0 < \theta < \frac{\pi}{2}$$

where the chirality $\chi = \pm 1$ stands for the handedness of the helix: $\chi = 1$ for a right-handed helix and $\chi = -1$ for a left-handed one [17]. The other filament of the plectoneme is obtained by a rotation of π about the helical axis \mathbf{e}_3 . The plectonemic region is characterized by the helical radius r and the helical angle θ , which are assumed to be independent of the arc length s . The complement $\pi/2 - \theta$ of the helical angle is often referred to as the pitch angle. Both r and θ may depend on the loading. Geometric impenetrability of the helices implies that $\theta \leq \pi/4$ [27,28]. Note that the external moment M_{ext} applied in the upper tail of the DNA molecule is equivalent to a total moment M_3 about \mathbf{r}'_p at the beginning of the plectonemic region. By the arguments of conservation of torque about the body axis of an isotropic rod, $\mathbf{m} \cdot \mathbf{d}_3 = K_t u_3 = M_3$ is a constant [24], implying that the twist u_3 is constant in the helical region.¹ One consequence of the use of the expressions given by Moroz and Nelson [26] is that the twist u_3 in the tails is different from that in the plectoneme even though the twisting moment $M_{ext} = M_3$ is the same, since the effective twist modulus is different in each region.

- At the end of the plectonemic region there is a loop. This end loop is formed in the transition from the straight configuration to the plectonemic configuration. In order to model the loop, we propose an approximation based on the localizing solution of an elastic rod [29,30], ignoring thermal fluctuations [31]. For details we refer the reader to Section S.1 of the supplementary data.

The molecule contour length spent per tail is denoted by l_t ($L_t = 2l_t$), the contour length in the loop is denoted by L_o and the contour length per helix is denoted by l_p ($L_p = 2l_p$). The sum of the length of all regions is given by $L = L_p + L_t + L_o$. The equilibrium configuration of the rod is fully specified by the centerline, through the variables r, θ and M_3 . In what follows, we compute these parameters as a function of the loading (the pulling force,

¹ At the transition point going from an initially straight state to a plectonemic state there is a jump in the external torque. We define $M_{ext} = M_{critical}$ as the twisting moment in the straight configuration right before the transition (no plectonemes formed), while $M_{ext} = M_3$ is defined as the twisting moment when plectonemes (helices) are present and $\delta M = M_{critical} - M_3$ as the jump in the twisting moment at the transition (see Section 3.1). We use the notation M_{ext} in Section 2 for the external torque. When plectonemes are present, the equations describing the DNA tails can be used by replacing M_{ext} with M_3 . When there are no plectonemes in the straight state right before the transition, the equations describing the DNA tails can be used to describe the entire molecule by replacing M_{ext} with $M_{critical}$.

F , and the number of turns, n) by minimizing the free energy of the system.

The experiments are performed under imposed end rotations; therefore, the energy minimization will be performed under the constraint that the number of turns n imposed on the bead at one end of the DNA is equal to the excess link Lk_p of the DNA molecule in the helical region, the excess link Lk_t in the tails and the excess link Lk_o in the loop:

$$n = Lk_p + Lk_t + Lk_o \quad (3)$$

where the link Lk_p in the helical region corresponds to the classical partition into twist Tw and writhe Wr [32]:

$$Lk_p = \left[\frac{M_{ext}}{2\pi K_t} - \chi \frac{\sin 2\theta}{4\pi r} \right] L_p \quad (4)$$

At this point, we note that clockwise rotations n about the \mathbf{e}_1 axis, corresponding to a positive external moment M_{ext} , generate a left-handed helix, with $\chi = -1$, while a negative external moment generates a right-handed helix, with $\chi = 1$. We also note that, in the presence of thermal fluctuations, there is a writhe contribution from the tails which can be accounted for by using the results of Moroz and Nelson [26]:

$$Lk_t = \frac{M_{ext}(L - L_p - L_o)}{2\pi} \left(\frac{1}{K_t} + \frac{1}{4K_b K} \right) + O(K^{-3}) \quad (5)$$

where

$$K = \frac{\sqrt{K_b F - M_{ext}^2/4}}{k_B T} \quad (6)$$

k_B is the Boltzmann constant and T is the absolute temperature. The link in the end loop can be approximated as (see Section S.1 of the supplementary data):

$$Lk_o = \frac{M_{ext} L_o}{2\pi K_t} + Wr_o \quad (7)$$

where $Wr_o \approx 1$ is the writhe present in the loop.

2.1. Potential energy of the system

It is convenient to express the total potential energy of the DNA filament as:

$$V = \int_0^L \Gamma(s, \theta, q_i) ds = V_{tails} + V_{loop} + V_{helices} \quad (8)$$

where q_i are variables like M_3, r, \dots independent of s . The free energy in the case of fixed force F and fixed-torque M_{ext} in the tails (straight portion) is given by [26]:

$$E_t = \left(-F - \frac{M_{ext}^2}{2K_t} + G_{flu}^* \right) L_t \quad (9)$$

where the last term is a correction due to thermal fluctuations:

$$G_{flu}^* = \frac{(k_B T)^2}{K_b} K \left(1 - \frac{1}{4K} - \frac{1}{64K^2} \right) + O(K^{-3}) \quad (10)$$

where K is given by Eq. (6). The extension with thermal fluctuations taken into account is given by $\partial E_t / \partial F = \rho L_t^2$, where

$$\rho = 1 - \frac{1}{2} \frac{1}{\sqrt{\frac{K_b F}{k_B^2 T^2} - \frac{M_{ext}^2}{4k_B^2 T^2} - \frac{1}{32}}} + \frac{K_b k_B T}{L_t \left(K_b F - \frac{M_{ext}^2}{4} \right)} \quad (11)$$

Slope of the rotation–extension curve after the formation of plectonemes can be obtained from constraint Eq. (3) together with

Eq. (11). The extension of the filament is given as $\Delta z = \rho(L - L_o - L_p)$. Noting that L is constant, L_o is approximately constant and ρ is independent of n , the overall slope of the rotation–extension curve is given by:

$$\frac{d}{dn}(\Delta z) = -\rho \frac{d}{dn}(L_p) \quad (12)$$

In what follows, we drop the negative sign and simply refer to the slope as $\rho(dL_p/dn)$. The end rotation conjugate to M_{ext} is given by $-\frac{\partial E_t}{\partial M_{ext}} = 2\pi Lk_t$. To get the free energy of the system under imposed end rotations Lk_t , we apply a Legendre transform:

$$V_{tails} = E_t + 2\pi Lk_t M_{ext} \quad (13)$$

The free energy of the loop will be approximated under the assumption that the bending and twisting energy decouple (see the supplementary data). The twisting moment M_{ext} is a constant along the molecule and therefore the twist energy per unit length is a constant too. The expression for the bending energy per unit length E_{o-bend} and the length of the loop L_o are obtained from the expressions given by Kúlic et al. [30] in the absence of twist:

$$V_{loop} = \left(\frac{M_{ext}^2}{2K_t} + E_{o-bend} \right) L_o \quad (14)$$

where $L_o = 4\sqrt{K_b/F}$ and $E_{o-bend} = F$.

The free energy of the plectonemic region can be divided into elastic energy $V_{el}^{helices}$ and the energy due to internal interaction $V_{int}^{helices}$. The elastic energy is given by:

$$V_{el}^{helices} = \left(\frac{K_b}{2} \kappa^2 + \frac{M_{ext}^2}{2K_t} \right) L_p \quad (15)$$

where $\kappa = \sin^2 \theta / r$ is the curvature of a uniform helix [24]. Eq. (15) captures the elastic behavior of the rod in response to the applied loadings; it is zero in the straight and twist less the (natural) configuration of the rod. The electrostatic and entropic interactions present in the plectonemic region $V_{int}^{helices} = U(r, \theta, x_i) L_p$ will be described in more detail later; here x_i represents any auxiliary parameters or internal variables that may appear in the free energy of the system depending on the model picked to describe the electrostatic and entropic parts of the energy. The potential energy can be written by separating the terms that contribute along L , and those that contribute only along L_p and L_o . We introduce a Lagrange multiplier λ to account for the constraint Eq. (3) and define:

$$I(\theta, r, M_3) = \frac{K_b \sin^4 \theta}{2r^2} + F + U(r, \theta, x_i) - G_{flu}^* - \frac{M_{ext}^2}{4K_b K} + \frac{\lambda}{2\pi} \left(\frac{M_{ext}}{4K_b K} + \chi \frac{\sin 2\theta}{2r} \right) \quad (16)$$

such that the final expression for the potential energy of the system subject to the constraint Eq. (3) is given by:

$$V = I(\theta, r, M_3) L_p + \left(\frac{M_{ext}^2}{2K_t} - F + G_{flu}^* + \frac{M_{ext}^2}{4K_b K} \right) L + \left(E_{o-bend} + F - G_{flu}^* - \frac{M_{ext}^2}{4K_b K} \right) L_o + \lambda \left[n - \frac{M_{ext} L}{2\pi} \left(\frac{1}{K_t} + \frac{1}{4K_b K} \right) + \frac{M_{ext} L_o}{8\pi K_b K} - Wr_o \right] \quad (17)$$

2.2. Internal energy: entropy and electrostatics

In the previous section we introduced the term $U(r, \theta, x_i)$ as a general expression to account for the internal interactions and configurational entropy cost in the plectonemic region. The term

² The given formula for ρ includes corrections as detailed in Moroz and Nelson [25].

$U(r, \theta, x_i)$ represents the undulation-enhanced free energy per unit length plus the electrostatic energy [33]. We split the internal energy of the plectoneme $U(r, \theta, x_i)$ into the configurational entropy cost contribution $U_{conf}(r, \theta, x_i)$ and the purely electrostatic interactions between the charged helices in ionic solution $U_{el}(r, \theta, x_i)$, such that $U = U_{conf} + U_{el}$.

2.2.1. Electrostatics

At moderate length scales, electrostatic interactions between phosphate groups in two different molecules and between phosphate groups and counterions (positively charged) and coions (negatively charged) are present in the solution. Theoretical analysis of electrostatic interactions between polyions in solution has been done by Kornyshev et al. [34] and Parsegian and co-workers [35,36]. To date, DNA-DNA interactions are still not clearly understood. We studied the effects of some variants of the internal energy models available in the literature that have been used to model DNA single-molecule experiments in Section S.2 of the supplementary data. One of the electrostatic models shown in Section S.2 is the Ubbink and Odjik [33] model derived for supercoiled DNA. This analytical model is based on the leading asymptotic contribution of the Debye-Huckel potential around two charged line segments (helices). The other model shown in Section S.2 of the supplementary data is the Marko and Siggia [37] electrostatic model. This model corresponds to a uniform approximation of the superposition of the potential in two limiting forms – the electrostatic potential independent of θ and the electrostatic potential independent of r . As noted by Ubbink and Odjik [33], this is less accurate. More importantly, since, in our problem, we are minimizing the free energy of the system, we are interested in the derivatives of the electrostatic potential. However, the Marko and Siggia superposition model underestimates the value of the derivative [33]. Finally, the Ubbink and Odjik model includes undulation enhancement effects due to thermal fluctuations. For these reasons, together with the results summarized in Section S.2 of the supplementary data, we have used the expression given by Ubbink and Odjik [33]:

$$U_{el} = U_{PB}(r, \theta, d_r) = \frac{1}{2} k_B T v^2 l_B g(\theta) \sqrt{\frac{\lambda_D \pi}{r}} e^{\frac{2q^2}{2} \frac{2r}{\lambda_D}},$$

$$g(\theta) = 1 + 0.83 \tan^2(\theta) + 0.86 \tan^4(\theta) \quad (18)$$

where d_r represents the small undulations of the helix in the radial direction and leads to a correction in the electrostatic interaction energy due to the thermal fluctuations. The Bjerrum length l_B (nm) is defined as the length scale at which thermal energy is equal to coulombic energy, and is approximately 0.7 nm in water at 300 K [38]. The Debye length λ_D (nm) and the effective linear charge v (nm^{-1}) depend on the monovalent salt concentration. It is important to note that no consensus has been reached on the exact value of v [18,21]. The Debye screening length in water can be obtained from $\lambda_D = 0.305[\text{nm}]/\sqrt{c_0[M]}$, where $c_0[M]$ is the monovalent salt concentration in molar units [38].

2.2.2. Configurational entropy

The fluctuation free energy is $k_B T$ per correlation region [37], and the free energy of entropic confinement per unit length of the strand in the plectonemic supercoil may be written approximately as a superposition of two fluctuating modes due to radial (d_r) and longitudinal ($p\pi$) displacements [33,39]:

$$U_{conf}(d_r, \theta) = \frac{k_B T}{A^{1/3}} \left[\frac{c_p}{(p\pi)^{2/3}} + \frac{c_r}{d_r^{2/3}} \right] \quad (19)$$

where $A = K_b/(k_B T)$ is the persistence length of the fluctuating rod. The term $2\pi p$ is the pitch of the helix and is given by $p = r \cot \theta$.

The terms c_r and c_p are in general unknown constants. For a worm-like chain confined in a harmonic potential, $c_r = c_p = 3(2^{-8/3})$ in one dimension [33], but, as noted by van der Maarel [39], it is not clear whether these values can be adopted for the supercoiled configuration. In our calculations in Section 3 we will use $c_r = c_p = 2^{-8/3}$, which are empirically optimized constants [39].

2.3. Variational formulation

Once the DNA has transitioned from the straight configuration into the plectonemic state, the external moment M_{ext} plateaus. Recall that we define $M_{ext} = M_3$ as the external moment present in the molecule in the plectonemic state. To minimize the energy, we need to equate the following partial derivatives to zero [16–19,33]:

$$\left\{ \frac{\partial V}{\partial M_3}, \frac{\partial V}{\partial r}, \frac{\partial V}{\partial \theta}, \frac{\partial V}{\partial L_p}, \frac{\partial V}{\partial d_r} \right\} = 0$$

which yields:

$$\lambda = 2\pi M_3 + O(K^{-3}) \quad (20)$$

$$\left(\frac{K_b \sin^4 \theta}{r^3} - \frac{\partial U(r, \theta)}{\partial r} + \chi M_3 \frac{\sin 2\theta}{2r^2} \right) L_p = 0 \quad (21)$$

$$\left(K_b \frac{2 \sin^3 \theta \cos \theta}{r^2} + \frac{\partial U(r, \theta)}{\partial \theta} + \chi M_3 \frac{\cos 2\theta}{r} \right) L_p = 0 \quad (22)$$

$$I(\theta, r, M_3) = 0, \quad (23)$$

$$\frac{\partial U(\theta, r, d_r)}{\partial d_r} = 0 \quad (24)$$

where $I(\theta, r, M_3)$ is given by Eq. (16). Note that we minimize with respect to the external moment M_3 , which is constant along the DNA molecule, instead of minimizing with respect to the twist u_3 [17,18], which is different in the tails and helices, depending on the magnitude of thermal motion. Because of the manner in which we treat fluctuations in the energy expressions, our results for the equilibrium supercoiling variables θ, r, M_3 do not depend on the value of K_b , unlike the case in the full solution in Neukirch and Marko [19]. We are interested in the non-trivial solution $L_p \neq 0$, which corresponds to the minimum energy configuration when $n > 0$. The results obtained in this section for the plectonemic state of the DNA molecule can also be obtained under the assumption that $L_0 \ll l$, when the loop size is neglected in comparison to the length of the tails and plectoneme.

3. Comparison with experiments and predictions: the complete model

We begin with a short review of the experiments. In Forth et al. [20], Brutzer et al. [4] and Mosconi et al. [6] the response of single DNA molecules to externally applied forces and torques was directly measured using an angular optical trap or magnetic tweezers. The end-to-end extension of the DNA molecule was monitored as a function of the number of turns n applied at the unconstrained end. Ma eo et al. [21] completed the data sets of the slopes in the experiments in Brutzer et al. [20] for 30, 60, 170 and 320 mM monovalent salt. Forth et al. [4] reported direct measurements of the external torque M_3 using optical traps, while Lipfert et al. [5] used a novel method to directly measure the torque in single-molecule experiments using magnetic tweezers. Both Brutzer et al. [20] and Mosconi et al. [6] provided indirect measurements of the external torques M_3 . Besides the experimental results, Ma eo et al. [21] also provided the external torque, radius and slopes of the rotation-extension curves from Monte Carlo simulations. The experimental data of the slopes from Brutzer et al. [20] matched quantitatively with the Monte Carlo results. Thus, Ma eo et al. [21] concluded that,

within a cylinder approximation, DNA–DNA interactions can be described only by a significantly reduced DNA charge. Ma et al. [21] derived a simple model which neglected the entropy due to thermal fluctuations in the DNA molecule and accounted for the electrostatic interactions using the Debye–Hückel equation for a point charge over two line segments (helices), where the effective linear charge ν is fitted to be 0.42 times the bare DNA charge (see the supplementary material in Ma et al. [21]).

The data sets from Brutzer et al. [20], Maffeo et al. [21] and Mosconi et al. [6] provide consistent slope values over the entire force range. The slopes from Forth et al. [4] are consistent with the rest of the data sets for moderate forces, but differ in magnitude at low forces, as shown in Figs. S.2.2 and S.6.1 of the supplementary data. In general, the experimental results confirmed that the slopes of the rotation–extension curves and the torques M_3 are both lower at higher salt concentrations. However, the various data sets show greater disagreement in the torque values (see Fig. S.6.2 of the supplementary data). The torque data sets from Forth et al. [4], Lipfert et al. [5] and Brutzer et al. [20] provide rather high M_3 values that do not agree quantitatively with the Monte Carlo simulations as functions of the salt concentration c_0 . For instance, the indirectly measured torque M_3 for the 320 mM series reported by Brutzer et al. [20] differs by about 20% from the ones obtained in the Monte Carlo simulations carried out by Ma et al. [21]. The torque measurements from Mosconi et al. [6] are the lowest and can be made consistent with the Monte Carlo simulations with a 1.5 pNnm offset. The indirect torque measurements of Mosconi et al. [6] and the force dependence of the slopes satisfy the “Maxwell”-type relation derived by Zhang and Marko [40], as do the simulations and our theory (see Section S.4 of the supplementary data). The values of M_3 reported by Forth et al. [4] at 150 mM are larger than the 50 mM series reported by Mosconi et al. [6] by more than 20% at low forces. This contradicts the general trend that at larger ionic concentrations the external torque should be lower [20,21], and provides an opportunity to determine what trends are predicted by theory.

In this section we compare our theoretical predictions to the different sets of data mentioned above. Since the electrostatics in DNA–DNA interactions is not completely understood and the different models in the literature have not reached consensus on the value of the effective linear charge ν , we will let it be a fitting parameter. Based on the work of Stigter [41–43], values ranging from 0.42 to 1 of the bare DNA charge (of a uniformly charged rod with radius $a \in [1,1.2]$ nm) are found in the literature [19,21,37]. Besides Stigter, Ubbink and Odijk [33] and Vologodskii and Cozzarelli [44] have also provided ν values for a charged cylinder with $a = 1.2$ nm. Our values of ν for each salt concentration lie within the range of values used by other authors. The effective linear charge ν used in our calculations (for each salt concentration) is presented in Table 1.

We show the results of our model, including the effect of undulations along the radial direction in the internal energy $U(r, \theta, d_r) = U_{PB}(r, \theta, d_r) + U_{conf}(\theta, d_r)$. The values of M_3, r and θ as functions of the external force F are obtained by solving the system of equations given by Eqs. 20, 21, 2, 23, 24. The slope can be obtained by combining Eqs. (3) and (12):

$$\frac{d\Delta z}{dn} = \rho \left[\frac{\sin 2\theta}{4\pi r} - \frac{M_3}{8\pi K_b K} \right]^{-1} \quad (25)$$

We have obtained solutions for F in a range of 0.4–3.5 pN, for which the Moroz and Nelson [26] formulae apply. In Figs. 2 and 3 we show the results of the present model under the conditions of the experiments in Brutzer et al. [20] and Ma et al. [21] for a DNA template of 1.9 kbp. In our calculations we use the bending modulus $K_b = 50k_B T$ nm as used by Brutzer et al. [20]. As seen in Figs. 2 and 3, the quantitative predictions of our model for

$M_3, d\Delta z/dn$ and r consistently match with the Monte Carlo simulations and experimental data in Ma et al. [21]. For low salt concentrations and high forces, the predictions of our theoretical model overestimate the external moments by only about 1 pNnm. It is reassuring that our theoretical model matches almost exactly the three variables $M_3, d\Delta z/dn$ and r with only one fitting parameter ν . We also found that the ratio of the undulations d_r to the superhelical radius r is about 30% which is consistent with the ratios reported by Ubbink and Odijk [33]. Similarly, in Fig. 2 we compare our theoretical predictions for the slope of the rotation–extension curves to some of the experimental data series reported by Mosconi et al. [6] for a DNA template of 15.9 kbp. As before, we pick ν to be a fitting parameter and use $K_b = 50k_B T$ nm. Fig. 2 shows excellent quantitative agreement between the direct measurement by Mosconi et al. [6] and our theoretical predictions. Our fitting values of ν (see Table 1) are consistent with each other and follow the expected trend by increasing as the salt concentration increases. Using the present internal energy model with the configurational entropy coefficients $c_r = c_p = 2^{-8/3}$ produces theoretical predictions for M_3 that follow the qualitative trend of the indirect measurements by Mosconi et al. [6] but differ quantitatively by about 2.5 pN (a possible reason for this discrepancy is given in Section S.4 of the supplementary data).

3.1. The transition point and jump estimates

It is known that at the transition from the straight to the plectonemic state there is a jump in the value of M_3 and the vertical extension of the DNA molecule [4,20,22]. The jump in the vertical extension means that a section of the initially straight DNA becomes a writhed supercoiled structure immediately after the transition. We define δn as the amount of twist from the straight configuration (right before the transition) which is transferred into writhe in the supercoiled configuration (after transition). Brutzer et al. [20] suggest, using a simple model to fit their data, that in the transition the amount of twist δn which is transferred into writhe is larger than $Wr_0 \approx 1$ by a significant amount (at $F = 3$ pN and $c_0 = 0.32$ M $\delta n = 1.6 \pm 0.1$ turns for the 1.9 kbp DNA template and $\delta n = 3.4 \pm 0.2$ turns for the 10.9 kbp DNA) [20]. This conclusion would suggest that the jump in their data corresponds to the formation of an initial loop and some helical turns. Hence, the jump in the end-to-end distance is not just the size of the end loop [20,22]. Strick et al. [45] show a measurement of the critical torque at the transition point based on the minimization of energy in an initial loop model. This calculation of $M_{Strick} = (2K_b F)^{1/2}$ is approximate since it ignores the thermal fluctuations in the loop and assumes that the loop is circular. As noted by Marko [46], the value of M_{Strick} overestimates the plectonemic torque data extracted from their MC simulations by 25%. Here we propose a different approach. The jump in the external moment is denoted by the difference $\delta M = M_{critical} - M_3$. We can estimate the critical number of turns $n_{critical}$ for which the transition occurs, the size of the jump in the end-to-end distance δz , and the jump δM by noting (i) that at the transition the energy of the straight configuration and plectonemic configuration are equal and (ii) that the linking number $n = Lk$ is a topological invariant that must be continuous at the transition between the two configurations. The energy of the straight configuration just before the transition is given by Eq. (13), replacing $M_{ext} = M_{critical}$ and $L_t = L$:

$$\hat{V}_s = \left(-F + \frac{M_{critical}^2}{2K_t} + G_{flu-s}^* + \frac{M_{critical}^2}{4K_s K_b} \right) L \quad (26)$$

where K_s and G_{flu-s}^* are given by Eqs. (6) and (10) evaluated at $M_{ext} = M_{critical}$. The energy of the plectonemic configuration just after the transition is given by Eq. (17), replacing $M_{ext} = M_3$:

Table 1

Effective linear charge ν used in our calculations as a function of the monovalent salt concentration c_o (mM). The third column shows the fraction $\xi = \nu/\nu_{bare}$, where ν_{bare} has been computed as in Refs. [19,41–43] for $a = 1$ nm. For salt concentrations in the range 30–500 mM, the value of the charge ν_{bare} can be approximated by a linear fit with $R^2 > 0.99$ (the linear fit predicts 99% of the variance on the fitted variable). Based on this idea, we performed a linear fit to the value of ν used and obtained $\nu^{fit} = 2.46 + 2.38 \times 10^{-2}c_o$, with $R^2 > 0.99$ and c_o in mM units. A linear fit to ξ gives $\xi^{fit} = 0.73 - 2.7 \times 10^{-4}c_o$. The fourth column shows the fraction $\tilde{\xi} = \nu/\nu_{bare}$, where ν_{bare} has been computed using $a = 1.2$ nm as in [21]. Note that for large salt concentrations ($c_o \sim 0.32 - 0.5[M]$) $\tilde{\xi} \approx 0.42$ is equal to the charge adaptation factor used in Maffeo et al. simulations [21].

c_o [mM]	ν [nm ⁻¹]	$\xi = \nu/\nu_{bare}$ ($a = 1$ nm)	$\tilde{\xi} = \nu/\nu_{bare}$ ($a = 1.2$ nm)
30	2.83	0.70	0.61
50	3.73	0.75	0.63
60	3.80	0.71	0.59
100	5.32	0.75	0.62
150	5.93	0.67	0.53
170	6.16	0.62	0.50
200	7.71	0.71	0.54
320	10.00	0.64	0.46
500	14.31	0.60	0.42

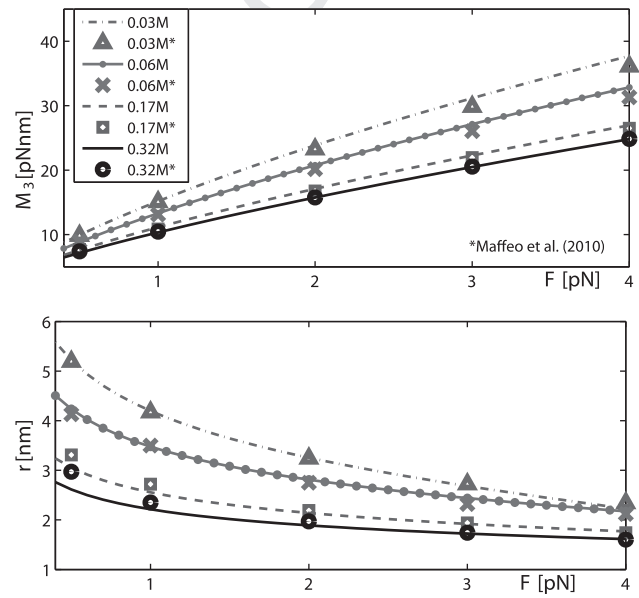
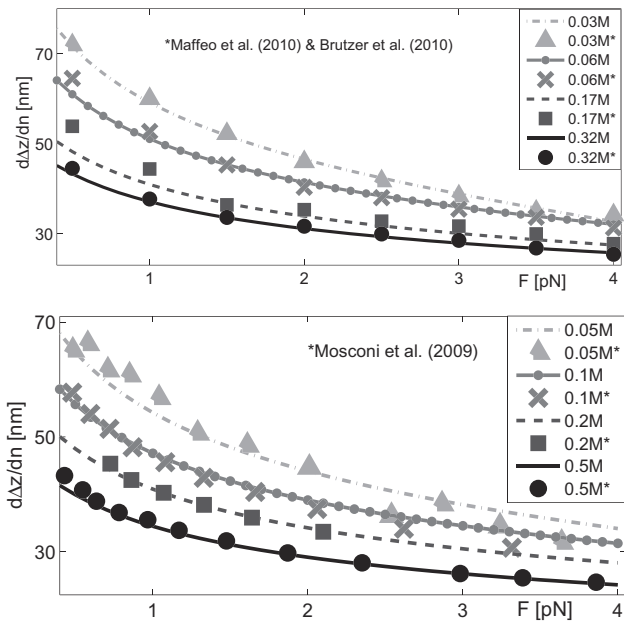


Fig. 2. Slope $d\Delta z/dn$ as a function of the external force F . Lines represent our predictions and markers the experimental data. The upper graph shows the experimental data in Brutzer et al. [20] and Maffeo et al. [21]. The values of the linear effective charge ν used are 2.83, 3.80, 6.16 and 10.00 nm⁻¹ for 30, 60, 170 and 320 mM salt concentration respectively. The lower graph shows the experimental data in Mosconi et al. [6], and the values of the linear effective charge ν used are 3.73, 5.32, 7.71 and 14.31 nm⁻¹ for 50, 100, 200 and 500 mM salt concentration respectively.

Fig. 3. External moment M_3 and superhelical radius r theoretical predictions for the different salt concentrations in Brutzer et al. [20]. The lines are our predictions and the markers are the data points corresponding to the values of r and M_3 in the Monte Carlo simulations of Maffeo et al. [21]. The values of ν used are shown in Table 1.

$$\hat{V}_p = \frac{M_3^2}{2K_t}L + \left(\frac{K_b \sin^4 \theta}{2r^2} + U \right) L_p^* + E_{o-bend}L_o + \left(G_{fluc-p}^* + \frac{M_3^2}{4K_bK_p} - F \right) (L - L_p^* - L_o) \quad (27)$$

where K_p and G_{fluc-p}^* are given by Eqs. (6) and (10), evaluated at $M_{ext} = M_3$. The length eaten by the helices during the transition due to the dynamic jump is L_p^* . Setting $\hat{V}_p = \hat{V}_s$, we get an equation with two unknowns $M_{critical}$ and L_p^* . We get a second equation by using the continuity requirement of $n = Lk$. In the straight DNA configuration, the critical number of turns n_{c-s} before the transition is given by:

$$n_{c-s} = \frac{M_{critical}}{2\pi}L \left(\frac{1}{K_t} + \frac{1}{4K_bK_s} \right) \quad (28)$$

In the plectonemic configuration, the critical number of turns n_{c-p} just after the transition is:

$$n_{c-p} = \frac{M_3L}{2\pi K_t} + \frac{M_3(L - L_p^* - L_o)}{8\pi K_bK_p} + Wr \quad (29)$$

where $Wr \approx 1 + \sin(2\theta)L_p^*/(4\pi r)$ accounts for the writhe present in the loop and the helices. Our second equation to solve for $M_{critical}$ and L_p^* is given by $n_{c-p} = n_{c-s}$. The amount of link (twist) that is converted into writhe is readily given from Eqs. (28) and (29) as the writhe after the transition minus the writhe before the transition:

$$\delta n = \left[\frac{M_3(L - L_p^* + L_o)}{8\pi K_bK_p} + Wr \right] - \left[\frac{M_{critical}L}{8\pi K_bK_s} \right] = \frac{\delta ML}{2\pi K_t} \quad (30)$$

From Eq. (30), if $\delta n \approx Wr \approx 1$, then we can conclude that only an end loop is formed and $L_p \approx 0$. Otherwise the jump in the end-to-end distance would correspond to the formation of an end loop and a plectonemic region of length L_p^* . Finally, the jump in the vertical extension is given by:

$$\delta z = \rho_s L - \rho_p \left[L - (L_p^* + L_o) \right] = \rho_p (L_p^* + L_o) + (\rho_s - \rho_p)L \quad (31)$$

where ρ_s and ρ_p correspond to Eq. (11) for ρ evaluated at $M_{ext} = M_{critical}$ and $M_{ext} = M_3$ respectively.

Next we show the results for the transition variables obtained using $K_t = 95k_B T$, which is an accepted value of the twisting modulus [15,26]. Our theoretical model predicts that the size of the jump at the transition strongly depends on the length of the DNA molecule and the salt concentration c_o . We find that the jump in the external moment δM decreases with increasing DNA length and the jump in the end-to-end extension δz increases with increasing DNA length. We conclude that, as c_o decreases, δM and δz decrease too. The experimental data in Forth et al. [4], Daniels et al. [22] and Brutzer et al. [20] agrees with our conclusion. Fig. 4 shows a comparison between the theoretical predictions and experimental measurements of $n_{critical}$ as a function of F , where we plot the solution for $n_{critical}$ accounting for an end loop. We also plot the solution obtained by ignoring the loop, by setting $Lk_o = Lk_p = 0$ in Eq. (3) and $L_p = L_o = 0$ in Eq. (5) such that the critical number of turns is given by $Lk_t = M_3 L [K_t^{-1} + (4K_b K_p)^{-1}] / (2\pi)$, similar to Clauvelin et al. [18]. The predicted $n_{critical}$ in the end loop model agrees very well with the data points from the experiments of Forth et al. [4] and Brutzer et al. [20], while ignoring the loop underestimates the values of $n_{critical}$. In Fig. 5 we show the comparison between the experimental measurements in Brutzer et al. [20] and Forth et al. [4] with our predictions for the jump in the end-to-end extension δz . Our qualitative predictions for the transition jump in the extension agree with experimental data, meaning that, as the DNA length L or c_o increases, so too does δz . As seen in Fig. 5, the experimental data from Brutzer et al. [20] and Forth et al. [4] show different trends as a function of the applied force F . We note that our theory predicts a relatively constant value of δz as a function of F for $c_o = 320$ mM (qualitatively similar to the experimental value) and describes qualitatively the decrease of δz as a function of F for $c_o = 150$ mM. In Section S.3 of the supplementary data we present a comparison of the predicted values of $M_{critical}$ with experimental data and also estimates of the torque jump δM .

We note that the numerical calculations of $n_{critical}$, L_p^* and $M_{critical}$ when comparing the energy of the two states ignore the fluctuation due to thermal kicks. An estimate of the fluctuations of n can be obtained within the Einstein approach for fluctuations [47,48]:

$$\langle \Delta n^2 \rangle = \frac{k_B T}{2\pi} \left. \frac{\partial n}{\partial M_{ext}} \right|_{T,F} \quad (32)$$

By so doing, we can approximate the change in the number of turns $\Delta n \approx \sqrt{\langle \Delta n^2 \rangle}$ due to the thermal kicks. Therefore the transition for a given force F takes place over $n_{critical}^{\pm k_B T} \approx n_{critical} \pm \Delta n$. For the cases presented in Fig. 4, $\Delta n \sim 0.5 - 1$ turns.

3.2. Coexistence of loops and plectonemes

Our methods also allow us to consider scenarios where we have a series of loops forming in the DNA instead of plectonemes. When only loops and no superhelical structures are present, the applied number of turns $n = Lk$ is distributed in the form of twist throughout the entire molecule, writhe due to thermal fluctuation in the straight regions [26] and writhe in the loops ($Wr_o \approx 1$ per loop formed). This happens when the energetic cost of forming a loop is lower than that of forming a writhed superhelix, and leads to a different slope of the rotation–extension curve. However, for a given choice of electrostatic and entropic interactions, we find that there is a range of forces in which the two regimes can coexist due to thermal motion.

The free energy per unit turn (excess link) in the plectonemic regime (see Eq. (17)) is:

$$V_{p\text{-turn}} = \frac{dL_p}{dn} \left[\frac{K_b}{2} k^2 + F + U - G_{flu}^* - \frac{M_3^2}{4K_b K_p} \right] = 2\pi M_3 \quad (33)$$

where $dL_p/dn = \rho^{-1}(d\Delta z/dn)$ given by Eq. (25). Since $Wr_o \approx 1$, the free energy per unit turn for a series of loops using the model described in the Section 2.1 is approximately:

$$V_{o\text{-turn}} \approx L_o \left[2F - G_{flu}^* - \frac{M_3^2}{4K_b K} \right] \quad (34)$$

Fig. 6 shows the regimes in which the free energy analysis would lead to the formation of either plectonemes or loops, or both. For moderate-to-high salt concentrations, $V_{p\text{-turn}} < V_{o\text{-turn}}$ for a range of external force [0.4,4] pN. As the salt concentration decreases, $V_{p\text{-turn}} \approx < V_{o\text{-turn}}$, and, due to thermal fluctuations, the two states could coexist. We have plotted the results for $c_o = 150$ mM and $c_o = 60$ mM. The lines on either side of the lower curve show the range $\pm k_B T$ at $T = 300$ K. If the upper curve is within $\pm k_B T$ of the lower curve, transitions between loops and plectonemes could occur. Recall that in our end-loop model we ignore self-contact, electrostatics and twist stored in the loop. Consequently, we expect that

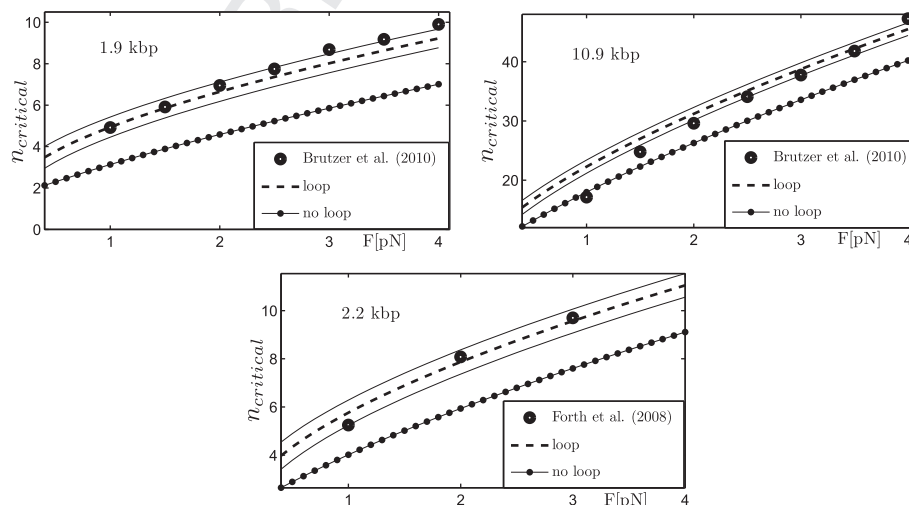


Fig. 4. Critical number of turns $n_{critical}$ as function of the external force. The lines represent our predictions and the markers show the experimental data. The experimental results were taken from Brutzer et al. [20] at $c_o = 320$ mM and Forth et al. [4] at $c_o = 150$ mM. For $c_o = 150$ mM we have used $\nu = 5.93$ nm⁻¹. Including the contribution of the end loop to compute $n_{critical}$ gives consistent results with the experiments. The thin continuous lines show the solution for $n_{critical} \pm \Delta n$ (including the end loop), where Δn is an estimate of the fluctuations in n during the transition.

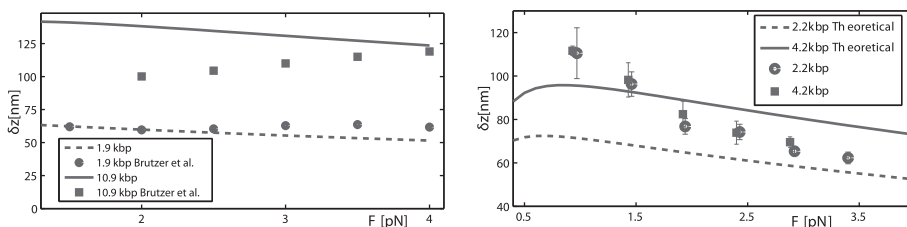


Fig. 5. Comparison of the extension jump δz from our theory with the experiments in Brutzer et al. [20] for 1.9 and 10.9 kbp DNA templates at $c_o = 320$ mM and the data in Forth et al. [4] for 2.2 and 4.2 kbp DNA templates at $c_o = 150$ mM. Our model predicts that, as the DNA length L or c_o increases, so does δz .

our analysis of the free energies per unit turn will give us only an estimate of the coexistence state of loops and plectonemes. We expect that, for moderate-to-high salt concentrations, plectonemes will be the favorable state, while for low-to-medium salt concentrations there might be a region of coexistence or even formation of only loops. Our predictions regarding the transition between the two states agree with the qualitative conclusion of Brutzer et al. [20].

3.3. Multivalent ions

In this section we extend our plectonemic DNA model to make predictions for DNA single-molecule experiments in the presence of multivalent ions. We consider the limiting case of a high concentration of monovalent ions and a low concentration of multivalent salt, as this is the case used in several experimental studies on DNA aggregation [49–51] and more recently in DNA single-molecule experiments (Q. Shao et al., private communication). These experiments show that the addition of small quantities of multivalent salt, such as spermidine Sp^{3+} or spermine Sp^{4+} , to a solution with a high monovalent salt concentration (0.2 M KCl) can modify the pitch and twist of the DNA plectoneme significantly. When the polyions are added to the solution the experiments yield more compact plectonemes, which start forming at lower values of the supercoiling density $\sigma_{critical} \approx 3.54(n_{critical}/L)$. The Debye length accounting for the different salts is given by [49]:

$$\lambda_{D-M}[nm] = 0.435[(\zeta^2 + \zeta)c_{mu}[M] + 2c_o[M]]^{-1/2} \quad (35)$$

where $c_{mu}[M]$ and $c_o[M]$ are the multivalent and monovalent salt concentrations in molar units, respectively, and ζ stands for the multivalent ion's valence. In the experiments of Dunlap and co-workers the control corresponds to a ~ 3 kbp DNA template at room temperature in a 0.2 M KCl salt solution. The experiments were performed with different concentrations of Sp^{3+} or Sp^{4+} added to the control. We have used $K_b = 55k_B T$ as measured in the experiments and $K_t = 95k_B T$. To compare with the experimental data, we fit the effective linear charge ν to the 0.6 pN point for each salt concentration and use it to predict the results for other values of the

force. Note that the experimental slopes of the rotation–extension curves from the 0.2 M KCl series of Dunlap and co-workers and the 0.2 M NaCl series in Mosconi et al. [6] do not agree quantitatively (see Fig. 7). In DNA molecular dynamic simulations by Savelev and Papoian [52], qualitative differences in Na^+ and K^+ condensation patterns were observed, suggesting that ion-specific modeling is required to describe electrostatics at short distances. In our plectonemic DNA model we account for the effects of ion-specific differences by the fitted value of ν . Table 2 shows the effective linear charge ν used in the calculations for a set-up consisting of $c_o = 0.2$ M KCl buffer with added multivalent salt (Sp^{3+} or Sp^{4+}) concentration c_{mu} .

Fig. 8 shows the comparison of our theoretical model and the experiment for Sp^{3+} , where we have plotted $d\Delta z^e/d\sigma$ as a function of the applied force F . $d\Delta z^e/d\sigma$ is the slope of the graphs showing the effective extension $\Delta z^e = \Delta z/L$ as a function of the degree of supercoiling $\sigma \propto n$. As the multivalent salt is increased, the plectonemes become more compact. This can be explained by better screening of the DNA charge by the salt solution (smaller ν value). The reduction in the value of ν with increased polyvalent salt has also been explained by the reduction in the electrophoretic charge value. The effective linear charge is proportional to α (electrophoretic charge value), as given by Stigter and co-workers [42,43]. For monovalent salt solutions, the value of α remains constant for a large range of concentrations [43], but this is not the case for polyvalent ions [54,55] or for mixtures of multivalent ions with monovalent salts [51].

For $c_{mu} = 5$ mM and $c_{mu} = 10$ mM, we found that, as the force F is increased, the supercoiling diameter approaches the interaxial distance ~ 3 nm found in hexagonally packed Sp^{3+} –DNA aggregates [49,53]. In aggregation and condensation experiments, the DNA formed close-packed hexagonal arrays, where the interaxial distance corresponded to an equilibrium spacing due to competition between the attractive and repulsive forces [53] that arise due to effects such as hydration, van der Waals forces, London-like dispersion forces and counter-ion fluctuations [54,53]. We expect that, as the polyvalent salt increases and the supercoiling diameter approaches 3 nm, these effects will become important and dominate the interactions, leading to compact DNA plectonemes with

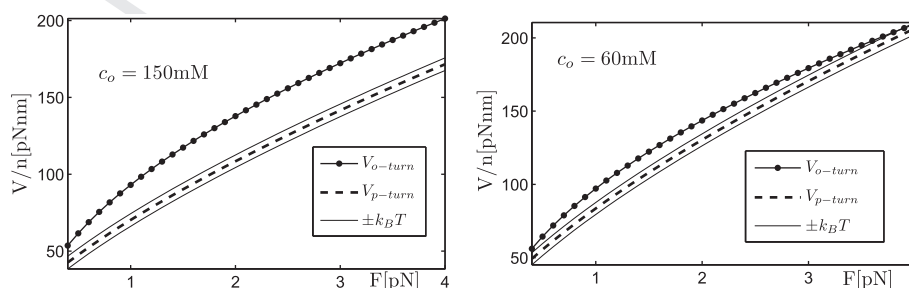


Fig. 6. Energy per unit turn. Using our model, we can get some idea of the preferred state: if $V_{o-turn} > V_{p-turn}$, plectonemes are favored; if $V_{p-turn} > V_{o-turn}$, loops are favored; and if $V_{o-turn} \approx V_{p-turn}$, there is a coexistence of loops and plectonemes. We expect that, for moderate-to-high salt concentrations, plectonemes will be formed, while for low-to-medium salt concentrations there might be a region of coexistence or even the formation of only loops.

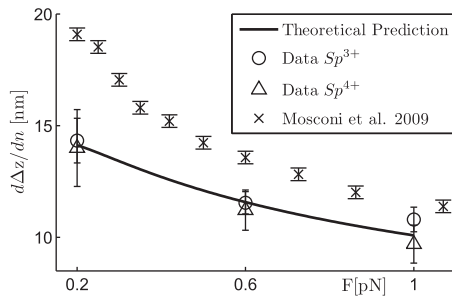


Fig. 7. Dunlap and co-workers performed two series of experiments corresponding to the control set-up ($c_0 = 0.2$ M KCl), one for spermidine Sp^{3+} (circles) and the other for spermine Sp^{4+} (triangles). We fit the value of ν to get the slope of the rotation–extension curve at $F = 0.6$ pN for the control set corresponding to Sp^{3+} (circles) and got $\nu = 4.12$ nm^{-1} . Our prediction with $\nu = 4.12$ nm^{-1} is shown by the solid line. The data from Mosconi et al. [6] shown by the cross markers corresponds to the $c_0 = 0.2$ M NaCl series.

Table 2

Effective linear charge ν for $c_0 = 0.2$ M KCl buffer and added multivalent salt concentration c_{mu} . For only the monovalent salt $c_0 = 0.2$ M KCl we used $\nu^0 = 4.12$ nm^{-1} . As the multivalent salt concentration is increased, the value of ν obtained from the fit decreases. This can be explained by a better screening of the DNA charge by the salt solution and the varying electrophoretic charge value in multivalent ion solutions. The Sp^{3+} values of ν are fitted well by the curve $\nu_{3+}^{fit} = \nu^0(1 + c_0/1.07)^{-1/3}$ ($R^2 > 0.97$), and the Sp^{4+} values of ν are fitted well by the curve $\nu_{4+}^{fit} = \nu^0(1 + c_0/0.07)^{-1/3}$ ($R^2 > 0.99$). The curve fits were obtained using the least squares method, with a fitting function of the form $f(x) = a/(b + x)^c$.

c_{mu} [mM] (Sp^{3+})	ν [nm^{-1}]	c_{mu} [mM] (Sp^{4+})	ν [nm^{-1}]
0	4.12	0.2	2.72
1	3.35	0.5	2.02
2	2.75	0.75	1.76
5	2.20	1	1.66
10	2.10	2	1.34

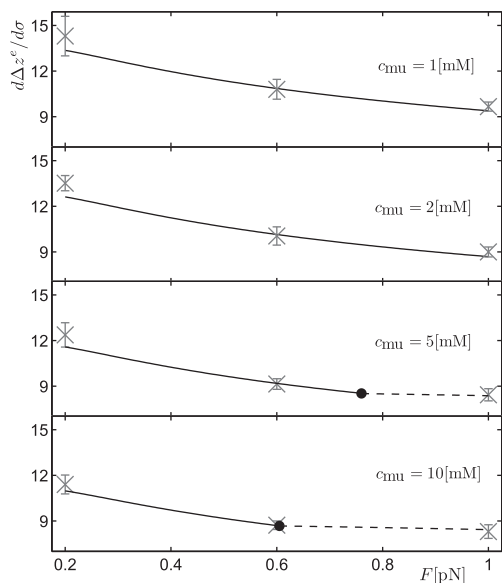


Fig. 8. Predictions for the slope of the rotation–extension curves in the presence of multivalent ions. Crosses are data points from Dunlap and co-workers for a mixture of $c_0 = 0.2$ M KCl and different c_{mu} concentrations of spermidine Sp^{3+} . For $c_{mu} = 5$ mM and $c_{mu} = 10$ mM, as F increases the supercoiling diameter decreases and approaches the interaxial spacing distance ~ 3.0 nm for spermidine [49,53]. The dot in the bottom two panels shows the point where $2r$ reaches the limiting interaxial distance, and from there on the dashed line shows the solution where $r = 1.5$ nm is assumed to be constant.

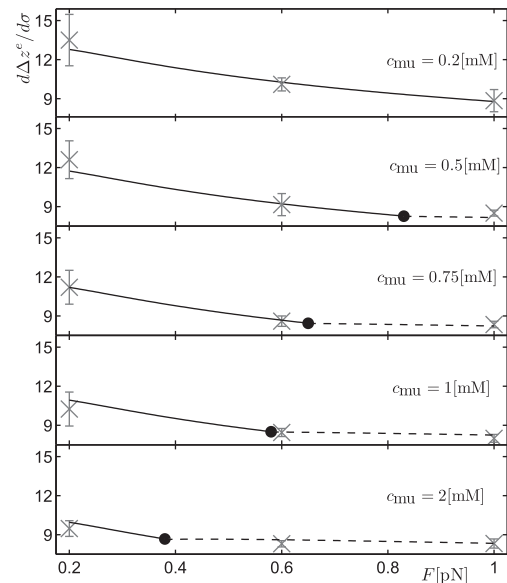


Fig. 9. Predictions of the slope of the rotation–extension curves in the presence of multivalent ions. Crosses are data points from Dunlap and co-workers for a mixture of $c_0 = 0.2$ M KCl and different c_{mu} concentrations of spermine Sp^{4+} . For $c_{mu} \geq 0.5$ mM, as F increases the supercoiling diameter approaches the interaxial spacing distance ~ 2.9 nm of spermine [49,53]. As in Fig. 8, the dot shows the point where $2r$ reaches the interaxial distance value, and the dashed line shows the solution where $r = 1.45$ nm is assumed to be constant.

a diameter approximately equal to the interaxial spacing. In Fig. 8 the dot shows the point where $2r = 3$ nm, and from there on the dashed line shows the solution for a constant $r = 1.5$ nm. Remarkably, our predictions with constant r match the experimental point at $F = 1$ pN for larger c_{mu} concentrations.

Fig. 9 show the results obtained when using spermine Sp^{4+} . For Sp^{4+} we have only fitted the value of ν to the experimental point $F = 0.6$ pN for the control set-up and $c_{mu} = 0.2 - 0.75$ mM concentrations, and obtained a curve for ν as a function of c_{mu} . For $c_{mu} = 1$ mM and $c_{mu} = 2$ mM, we have extrapolated the value of ν from the curve obtained from the previous fitted values. As before, the dot shows the point where $2r$ is equal to the interaxial spacing ~ 2.9 nm for Sp^{4+} (Raspaud et al. [53], Todd et al. [49]), and from there on the dashed lines correspond to the solution with $2r \approx 2.9$ nm. Our results for both types of polyvalent ions show good quantitative agreement with the experimental values. In Section S.5 of the supplementary data we show that our results are in good agreement with experimental measurements of the supercoiling density $\sigma_{critical}$ at which the DNA molecule makes the transition from the straight to the supercoiled configuration. The theoretical predictions of the plectonemic moment M_3 and supercoiling radius r can also be found in Section S.5 of the supplementary data.

4. Conclusions

We have analyzed the mechanics of plectoneme formation, where a twisted DNA molecule in the plectonemic regime has been modeled as an elastic–isotropic rod. Here we give a short summary of all the results we have obtained. We have used a variational approach to solve the energy minimization problem that corresponds to angular optical trap (or magnetic tweezers) experiments on a DNA molecule attached to a substrate at one end, while subjected to a tensile force and twisted by a specific number of turns n at the other end [4–6,20]. Our model description is symmetric, in that over-twisting and under-twisting the rod under tension give

the same results. However, this is not the case in DNA for a large number of turns n (or supercoiling density σ). Stretching and under-twisting DNA at low-to-moderate values of σ leads to denaturation, as is known from experiment [45] and atomistic simulations [56]. Therefore, our model is valid in the over-twisting regime only for moderately large values of σ (before a structural transition into P-DNA [57]), where the Moroz and Nelson [26] formulae are valid and the DNA can be modeled with constant elastic properties along the entire molecule. We have minimized the energy with respect to the dependent variable M_{ext} rather than its conjugate n , since we are modeling rotation controlled experiments. We do not minimize with respect to the twist u_3 , since M_{ext} is constant along the DNA molecule while u_3 is different in the tails and the helices, depending on the magnitude of thermal motion. An interesting, and possibly experimentally verifiable, result of minimizing with respect to M_{ext} is that the equilibrium supercoiling variables θ, r and M_3 are only functions of the bending modulus K_b , but are independent of the twisting modulus K_t .

In our one-dimensional continuum description of the DNA molecule we account for DNA elasticity, DNA–DNA interactions, fluctuations and configurational entropy in the tails and helices. As mentioned before, there is no consensus on the electrostatic models in the mechanics of DNA. We thus used our theoretical framework to test several models of DNA–DNA electrostatic interactions and configurational entropy in the plectonemic region (see Section S.2 of the supplementary data). Understanding the effects of each of the models and approximations ultimately led us to pick the $U(r, \theta, d_r)$ model of Ubbink and Odijk [33], with the entropic parameters $c_p = c_r$ given by van der Maarel [39]. The electrostatic contribution to K_b is rather small for the physiological range (0.1–0.5 M) of salt concentrations [58,59]. Therefore, both the bending and configurational entropy energetic costs are independent of the salt concentration. Hence, for a given monovalent salt, the plectonemic configuration as a function of F is dictated by ν . So, as noted by Ma eo et al. [21], single-molecule experiments can be used to determine the appropriate effective linear charge ν for plectonemic DNA. Here we give simple analytical formulae for ν as a function of salt concentration for both monovalent and some multivalent salts (in low concentrations) that result in strong agreement of our analytical model with the different sets of experimental data and Monte Carlo simulations over a wide range of forces. Our qualitative results agree with the conclusions obtained in previous works [15–19,21], and the values of ν are within the range previously obtained by others. As the salt concentration increases, the charge adaptation factor ν/ν_{bare} decreases (see Table 1), and the reduced effective linear charge ν approaches the values used in the simulations of Maffeo et al. [21].

In our model we have also accounted for the presence of the end loop. This allows us to compare the energy of the straight DNA configuration and the plectonemic DNA, and leads to a method to obtain analytical estimates of the jumps in the external torque δM and end-to-end extension δz of the DNA molecule at the transition. Our predictions of the jump variables and the critical number of turns at which the transition occurs agree with those observed experimentally. If the energetic cost of forming a loop is lower than that of forming a helix, then we will have a series of loops, and this will lead to a different slope of the rotation–extension curve. However, there is a range of ionic concentrations and forces at which the two regimes can coexist due to thermal motion. We have concluded that at moderate-to-high salt concentrations the most favorable state is the plectoneme, but as the salt concentration decreases the energy difference between a loop and a plectoneme also decreases. In our model we have assumed that the plectonemes can be modeled as uniform helices with constant radius and curvature. This does not have to be the case, and softening the constraints in the model might lead to a better understanding

of the problem. For instance, allowing the helical axis of the plectoneme to bend could lead to more complicated structures. Further, since constant curvature solutions require special boundary conditions, we consider it important to analyze the more general case of variable curvature solutions [60]. Variable curvature solutions can provide theoretical insight into the formation of multiple plectonemes because for two (or more) interwound helices there is a geometrical lock-up helical angle [27].

Finally, we have shown that our model for plectonemic DNA including the end loop can reproduce experimental data from single DNA molecule experiments in the presence of polyvalent ions. The theoretical estimates of the slopes and critical number of turns ($n_{critical} \propto \sigma_{critical}$) match experiments (D. Dunlap, private communication) where low concentrations of multivalent salts are added to a high concentration of monovalent salt solution. In the presence of multivalent ions, it is well known that DNA forms toroidal condensates in bulk [61], and recently toroids have been suspected to form when DNA is subjected to a tensile force [62]. A potential field of study is complex DNA condensates due to polyvalent ions in the presence of forces and torsional constraints, where there could be formation of plectonemes and toroids alike.

Acknowledgements

We acknowledge partial support through an NSF CAREER award, Grant No. NSF CMMI-0953548, and from the Nano/Bio Interface Center at the University of Pennsylvania through Grant No. NSF DMR08-32802. We thank Qing Shao, Sachin Goyal, Laura Finzi and David Dunlap at Emory University for providing us with their experimental data and for discussions.

Appendix A. Supplementary data

S.1: The end loop; S.2: Testing the Internal Energy models; S.3: Critical Torque Mcritical and the jump M Mcritical M3; S.4: Indirect method for calculating external moment; S.5: Multivalent Ions; S.6: Experimental and simulation data. Supplementary data associated with this article can be found, in the online version, at doi:10.1016/j.actbio.2012.01.030.

References

- [1] Nelson P. Biological physics. New York: W.H. Freeman and Company; 2004.
- [2] Koster D, Croquette V, Dekker C, Shuman S, Dekker N. Friction and torque govern the relaxation of DNA supercoils by eukaryotic topoisomerase IB. Nature 2005;434:671–4.
- [3] Koster D, Crut A, Shuman S, Bjornsti M, Dekker N. Cellular strategies for regulating DNA supercoiling: a single-molecule perspective. Cell 2010;142(4):519–30.
- [4] Forth S, Deufel C, Sheinin MY, Daniels B, Sethna JP, Wang D. Abrupt buckling transition observed during the plectoneme formation of individual DNA molecules. Phys Rev Lett 2008;100(14):148301.
- [5] Lipfert J, Kerssenmakers J, Jager T, Dekker N. Magnetic torque tweezers: measuring torsional stiffness in DNA and RecA-DNA filaments. Nat Methods 2010;Published online doi:10.1038/nmeth.1520, [17 October 2010].
- [6] Mosconi F, Allemand J, Bensimon D, Croquette V. Measurement of the torque on a single stretched and twisted DNA using magnetic tweezers. Phys Rev Lett 2009;102(7):078301.
- [7] Strick T, Allemand J, Bensimon D, Bensimon A, Croquette V. The elasticity of a single supercoiled DNA molecule. Science 1996;271(5257):1835–7.
- [8] Strick T, Dessinges MN, Charvin G, Dekker N, Allemand JF, Bensimon D, et al. Stretching of macromolecules and proteins. Rep Prog Phys 2003;66(1):1–45.
- [9] Fraser W, Stump D. The equilibrium of the convergence point in two-strand yarn plying. Int J Solid Struct 1998;35(3–4):295–8.
- [10] Coleman B, Swigon D. Theory of supercoiled elastic rings with self-contact and its application to DNA plasmids. J Elasticity 2000;60:173–221.
- [11] Thompson J, van der Heijden G, Neukirch S. Supercoiling of DNA plasmids: mechanics of the generalized ply. Proc R Soc Lond A 2002;458(2020):959–85.
- [12] Goyal S, Perkins N, Lee C. Nonlinear dynamics and loop formation in Kirchhoff rods with implications to the mechanics of DNA and cables. J Comput Phys 2005;209(1):371–89.
- [13] Goyal S, Perkins N. Looping mechanics of rods and dna with non-homogeneous and discontinuous stiffness. Int J Non-Linear Mech 2008;43:1121–9.

- [14] van der Heijden G, Thompson J, Neukirch S. A variational approach to loaded ply structures. *J Vib Control* 2003;9(1-2):175–85.
- [15] Purohit PK. Plectoneme formation in twisted fluctuating rods. *J Mech Phys Solids* 2008;56(5):1715–29.
- [16] Purohit P.K. Shape and energetics of DNA plectonemes. Chapter in IUTAM book series: IUTAM Symposium on Cellular, Molecular and Tissue Mechanics; 2010. ISBN 978-90-481-3347-5.
- [17] Clauvelin N, Audoly B, Neukirch S. Mechanical response of plectonemic DNA: an analytical solution. *Macromolecules* 2008;41(12):4479–83.
- [18] Clauvelin N, Audoly B, Neukirch S. Elasticity and electrostatics of plectonemic DNA. *Biophys J* 2009;96(9):3716–23.
- [19] Neukirch S, Marko J. Analytical description of extension, torque, and supercoiling radius of a stretched twisted DNA. *Phys Rev Lett* 2011;106(13):138104.
- [20] Brutzer H, Luzziotti N, Klaue D, Seidel R. Energetics at the DNA supercoiling transition. *Biophys J* 2010;98(7):1267–76.
- [21] Maffeo C, Robert S, Brutzer H, René S, Aleksei A, Gero W, et al. DNA-DNA interactions in tight supercoils are described by a small effective charge density. *Phys Rev Lett* 2010;105(15):158101.
- [22] Daniels B, Forth S, Sheinin MY, Wang D, Sethna JP. Discontinuities at the DNA supercoiling transition. *Phys Rev E* 2009;80:040901. R.
- [23] Chouaieb N, Goriely A, Maddocks J. Helices. *Proc Natl Acad Sci* 2006;103(25):9398–403.
- [24] van der Heijden G. The static deformation of a twisted elastic rod constrained to lie on a cylinder. *Proc R Soc Lond A* 2001;457(2007):695–715.
- [25] Moroz J, Nelson P. Torsional directed walks, entropic elasticity, and DNA twist stiffness. *Proc Natl Acad Sci* 1997;94(26):14418–22.
- [26] Moroz J, Nelson P. Entropic elasticity of twist-storing polymers. *Macromolecules* 1998;31(18):6333–47.
- [27] Stasiak A, Maddocks J. Mathematics. Best packing in proteins and DNA. *Nature* 2000;406(6793):251–3.
- [28] Pierański P. In: search of ideal knots. Series on Knots and everything, vol. 19. Singapore: World Scientific; 1998. p. 20–41.
- [29] Coyne J. Analysis of the formation and elimination of loops in twisted Cable. *IEEE J Oceanic Eng* 1990;15:72–83.
- [30] Kúlic IM, Mohrbach H, Thaokar R, Schiessel H. Equation of state of looped DNA. *Phys Rev E* 2007;75(1):011913.
- [31] Agrawal NJ, Radhakrishnan R, Purohit P. Geometry of mediating protein affects the probability of loop formation in DNA. *Biophys J* 2008;94:3150–8.
- [32] Neukirch S, Starostin EL. Writhe formulas and antipodal points in plectonemic DNA configurations. *Phys Rev E* 2008;78(4):041912.
- [33] Ubbink J, Odijk T. Electrostatic-undulatory theory of plectonemically supercoiled DNA. *Biophys J* 1999;76(5):2502–19.
- [34] Kornyshev AA, Lee DJ, Leikin S, Wynveen A. Structure and interactions of biological helices. *Rev Mod Phys* 2007;79(3):943–96.
- [35] Brenner S, Parsegian V. A physical method for deriving the electrostatic interaction between rod-like polyions at all mutual angles. *Biophys J* 1974;14(4):327–34.
- [36] Podgornik R, Parsegian V. Molecular fluctuations in the packing of polymeric liquid crystals. *Macromolecules* 1990;23(8):2265–9.
- [37] Marko J, Siggia E. Statistical-mechanics of supercoiled DNA. *Phys Re E* 1995;52(3):2912–38.
- [38] Andelman D. Introduction to electrostatics in soft and biological matter. In: Scottish Graduate Series. Boca Raton, FL: Taylor and Francis; 2006. p. 97–122.
- [39] van der Maarel JRC. Introduction to biopolymer physics. Singapore: World Scientific; 2008.
- [40] Zhang H, Marko J. Maxwell relations for single-DNA experiments: Monitoring protein binding and double-helix torque with force-extension measurements. *Phys Rev E* 2008;77(3 Pt 1):031916.
- [41] Stigter D. The charged colloidal cylinder with a Gouy double layer. *J Colloid Interface Sci* 1975;53:296.
- [42] Stigter D. Interactions of highly charged colloidal cylinders with applications to double-stranded DNA. *Biopolymers* 1977;16:1435–48.
- [43] Schellman J, Stigter D. Electrical double layer, zeta potential, and electrophoretic charge of double-stranded DNA. *Biopolymers* 1977;16:1415–34.
- [44] Vologodskii A, Cozzarelli N. Modeling of long-range electrostatic interactions in DNA. *Biopolymers* 1995;35(3):289–96.
- [45] Strick T, Allemand J, Croquette V, Bensimon D. Twisting and stretching single DNA molecules. *Prog Biophys Mol Biol* 2000;74(1-2):115–40.
- [46] Marko J. Torque and dynamics of linking number relaxation in stretched supercoiled DNA. *Phys Rev E* 2007;76(2):021926.
- [47] Rudoï Y, Sukhanov A. Thermodynamic fluctuation within the Gibbs and Einstein approaches. *Usp Fiz Nauk* 2000;43(12):1169–99.
- [48] Landau LD, Lifshitz EM. Statistical Physics. 3rd ed. New York: Pergamon Press; 1980. Pt. 1.
- [49] Raspaud E, Durand D, Livolant F. Interhelical spacing in liquid crystalline spermine and spermidine–DNA precipitates. *Biophys J* 2005;88:392–403.
- [50] Burak Y, Ariel G, Andelman D. Competition between condensation of monovalent and multivalent ions in DNA aggregation. *Curr Opin Colloid Interface Sci* 2004;9:53.
- [51] Besteman K, van Eijk K, Lemay S. Charge inversion accompanies DNA condensation by multivalent ions. *Nat Phys* 2007;3:641.
- [52] Savelyev A, Papoian G. Inter-DNA electrostatics from explicit solvent molecular dynamics simulations. *J Am Chem Soc* 2007;129:6060–1.
- [53] Todd B, Parsegian V, Shirahata A, Thomas T, Rau D. Attractive forces between cation condensed DNA double helices. *Biophys J* 2008;95:4775–82.
- [54] Sottas P, Larquet E, Stasiak A, Dubochet J. Brownian dynamics simulation of DNA condensation. *Biophys J* 1999;77:1858–70.
- [55] Luan B, Aksimentiev A. Electric and electrophoretic inversion of the DNA charge in multivalent electrolytes. *Soft Matter* 2010;6:243–6.
- [56] Lughton CA, Harris SA. Atomistic simulation of DNA. *Atomistic simulation of DNA* 2011;1:6590–600.
- [57] Bryant Z, Stone M, Gore J, Smith SB, Cozzarelli N, Bustamante C. Structural transitions and elasticity from torque measurements on DNA. *Nature* 2003;424:338–41.
- [58] Noy A, Golestanian R. The chirality of DNA: elasticity cross-terms at base-pair level including A-tracts and the influence of ionic strength. *J Phys Chem B* 2010;114:8022–31.
- [59] Baumann CG, Smith SB, Bloomfield VA, Bustamante C. Ionic effects on the elasticity of single DNA molecules. *Proc Natl Acad Sci USA* 1997;94:6185–90.
- [60] Purohit PK, Argudo DE. Plectonemes with non-uniform helical pitch in single molecule DNA experiments. In Proceedings of the 7th European Nonlinear Dynamics Conference (ENOC 2011); 2011. doi:10.3267/ENOC2011Rome.
- [61] Brewer L. Deciphering the structure of DNA toroids. *Intgr Biol* 2010;published online doi:10.1039/c0ib00128g.
- [62] Battle C, van den Broek B, Noom M, van Mameren J, Wuite G, MacKintosh F. Visualizing the formation and collapse of DNA toroids. *Phys Rev E* 2009;80:031917.

Supporting Information : The dependence of DNA supercoiling on solution electrostatics

David Argudo and Prashant K. Purohit*

*Department of Mechanical Engineering and Applied Science, University of Pennsylvania,
Philadelphia PA 19104 USA*

E-mail: purohit@seas.upenn.edu

Phone: 215-898-3870. Fax: 215-573-6334

S.1 The end loop

At one end of the plectoneme there is a loop. The end loop is formed in the transition from the straight DNA configuration to a plectonemic DNA configuration. In the classical theory, the loop is formed when a rod subjected to tension and twist (applied number of turns) undergoes localized buckling at a critical torque $2\sqrt{K_b F}$ [1–3] up to a point where there is a dynamic jump into self-contact. The localized solution to the equilibrium equations of the rod is unstable, and consequently the perturbed rod jumps dynamically either to the straight rod or the loop configuration with self-contact [2, 4]. Formulations of the rod with contact points have been studied for both closed and open rods with applications to DNA supercoiling [5, 6]. As pointed out by Daniels et al.[7] in the DNA case, the transition happens due to free energy minimization and not due to instability or buckling. Due to thermal fluctuations the system can be perturbed sufficiently to go from the straight configuration into a lower and stable energetic state, which for a given applied torque

*To whom correspondence should be addressed

M_{ext} (number of turns n), we predict to be the plectonemic state. So a DNA strand subjected to tension and controlled number of turns does not reach the classical critical buckling torque $2\sqrt{K_b F}$, and hence $M_{critical} < 2\sqrt{K_b F}$. The jump in the external moment can be characterized as the difference $\delta M = M_{critical} - M_3$, where M_3 is the torque in the plectonemic state. Strick et al.[8] show a measurement of the critical torque at the transition point based on the minimization of energy of an initial (circular) loop model. This calculation of $M_{critical} = (2K_b F)^{1/2}$ is approximate since it neglects the thermal fluctuations in the loop and assumes a circular geometry. We propose a better approximation to account for the end loop based on a localizing solution of the rod. To our knowledge the energy stored in the loop derived from an analysis including bending, twist and thermal fluctuation has not yet been carried out. Coyne [1] analyzed the formation of loops in twisted semi-infinite rods, providing expressions for the energy of the buckled-loop configuration without self-contact. In the limit when $M_{ext} = 0$, the Coyne expressions reduce to the expressions given by Kúlic et al.[9] without thermal fluctuations. We will assume that thermal fluctuations are negligible in the end loop [10]; this is a good approximation when the loop has small average radius of curvature. In the case of the planar homoclinic loop under tension with no moment applied at the ends, Kúlic et al. [9] show that the expressions for the free energy in the straight plus loop and straight configurations differ by an amount equal to the elastic energy present in the loop. Their result is given below and takes into account both the bending energy and the work against the end force F :

$$E_{loop} = (E_{o-bend} + F)L_o = 8\sqrt{K_b F} = 2FL_o \quad (\text{S.1.1})$$

where $L_o = 4\sqrt{\frac{K_b}{F}}$. In the absence of thermal fluctuations, but including twist, the free energy of the loop (E_{loop}) is given by [1, 3]:

$$E_{loop} = \left(\frac{M_{ext}^2}{2K_t} + E_{o-bend} + F \right) L_o, \quad (\text{S.1.2})$$

where

$$E_{o-bend} = F, \quad L_o = 4\sqrt{\frac{K_b}{F}} \left(1 - \frac{M_{ext}^2}{4K_b F} \right)^{1/2}.$$

The expression for the writhe present in the loop is [3]:

$$Wr_o = \frac{2}{\pi} \cos^{-1} \left(\frac{M_{ext}}{2\sqrt{K_b F}} \right). \quad (\text{S.1.3})$$

The expressions for E_{o-bend} and Wr_o that we pick have to satisfy the condition that the number of turns $2\pi n$ is conjugate to the applied torque M_{ext} . We see that $Wr_o = 1$ only for $M_{ext} = 0$, becoming a planar homoclinic loop as in the case analyzed by Kúlic et al. [9]. Based on this idea we will approximate the energy of the loop by decoupling the bending and twisting energy, such that the E_{o-bend} and L_o are given by Kúlic et al. [9] formulae and the twist energy of the loop is the first term in (Eq. (S.1.2)).

S.2 Testing the Internal Energy models

In Clauvelin et al. [11] the mechanical description is combined with different analytical theories of DNA-DNA interactions that can be found in literature. The work in Clauvelin et al. [11] picked two well established models. The first is U_{PB} , derived by Ubbink and Odijk [12] from the Poisson-Boltzman equation; the second is U_{cc} , derived by Manning [13] and is based on the counterion condensation theory. According to the results obtained in Clauvelin et al. [11], an approximation of $U_{PB}(r, \theta)$ provided better agreement with experiment. When the undulations in the radial direction are not restrained by electrostatics but only by the structure of the plectoneme, the variable d_r will not appear in the electrostatic expression $U_{PB}(r, \theta)$ [11]:

$$U_{PB}(r, \theta) = \frac{1}{2} k_B T v^2 l_B g(\theta) \sqrt{\frac{\lambda_D \pi}{r}} e^{-\frac{2r}{\lambda_D}},$$

$$g(\theta) = 1 + 0.83 \tan^2(\theta) + 0.86 \tan^4(\theta). \quad (\text{S.2.1})$$

Similarly r will replace d_r in the configurational entropy expression given by Ubbink and Odijk [12] as done in Marko and Siggia[14]:

$$U_{conf-MS}(r, \theta) = \frac{k_B T}{A^{1/3}} \left[\frac{1}{(p\pi)^{2/3}} + \frac{1}{r^{2/3}} \right], \quad (\text{S.2.2})$$

where the constants $c_r = c_p = 1$. Additionally, Marko and Siggia [14] developed an analytical model for the electrostatic interactions that has also been used in the study of DNA single molecule experiments [15, 16]. The expression for the Marko and Siggia electrostatic model $U_{MS}(r, \theta)$ is:

$$U_{MS}(r, \theta) = l_B k_B T \nu^2 \left[K_0 \left(\frac{2r}{\lambda_D} \right) + K_0 \left(\frac{\pi r \cot \theta}{\lambda_D} \right) \right], \quad (\text{S.2.3})$$

where $K_0(x)$ is the modified Bessel function of the second kind. Table S.2.1 summarizes the different models used to described the internal energy interactions in our calculations, showing the figures where each one of them has been used in this section of the Supporting Information.

Table S.2.1: Internal Energy Models

Label	Model	Figures
U_1	$U_{PB}(r, \theta) + U_{conf-MS}(r, \theta)$	Figure S.2.1, Figure S.2.2
U_2	$U_{MS}(r, \theta) + U_{conf-MS}(r, \theta)$	Figure S.2.1
U_3	$U_{PB}(r, \pi/6) + U_{conf-MS}(r, \pi/6)$	Figure S.2.1
U_4	$U_{PB}(r, \theta, d_r) + U_{conf}(\theta, d_r)$	Figure S.2.2, Figure S.2.3
U_5	$U_{PB}(r, \theta)$	Figure S.2.2

We obtain theoretical results under the experimental conditions of Forth et al. [17]. The experiments were performed in phosphate buffered saline with 150 mM NaCl at 23.5°C. Numerical calculations resembling the experiments were performed assuming $K_b = 50k_B T$ and $K_t = 95k_B T$. The values used for the electrostatic parameters are:

- The Bjerrum length is $l_B \approx 0.715$ nm [12].
- The Debye length $\lambda_D \approx 0.8$ nm.
- The effective charge $\nu = 8.06$ nm⁻¹, where an interpolation of values listed in Table 7 in

Ubbink and Odijk [12] has been used. In the main text the effective linear charge ν is treated as a fitting parameter.

Internal energy models: effects and comparison

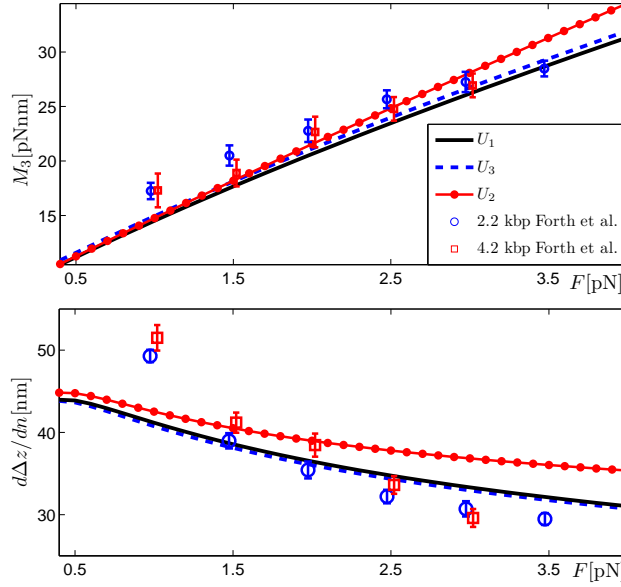


Figure S.2.1: Comparison between the solutions based on different internal energy models under the experimental conditions of Forth et al. [17]. The black solid line uses $U_1 = U_{PB}(r, \theta) + U_{conf-MS}(r, \theta)$, the red dotted line uses $U_2 = U_{MS}(r, \theta) + U_{conf-MS}(r, \theta)$ and the blue dashed line uses $U_3 = U_{PB}(r, \pi/6) + U_{conf-MS}(r, \pi/6)$ which is a function only of r . The value of the effective linear charge used is $\nu=8.06$ [nm^{-1}].

We show in Figure S.2.1 a comparison of the results obtained using Marko and Siggia's $U_2(r, \theta)$ electrostatic model with variants of the Poisson-Boltzmann model: $U_1(r, \theta)$ and $U_3(r, \pi/6)$.

The helical angle θ , using the U_1 and U_2 models, increases slightly as a function of the applied force F and it is approximately equal to $\pi/6$ for large forces, while the helical radius r decreases as a function of F and approaches the crystallographic radius 1nm (not shown). Since θ does not vary dramatically as a function of the applied force note that the curves obtained using the approximation $U_3(r) = U_{PB}(r, \pi/6) + U_{conf-MS}(r, \pi/6)$ are very close to those obtained from the internal energy models with θ dependence. Using $\theta = 0$, where the angle dependence is neglected as done in Clauvelin et al.[11, 18] and Neukirch and Marko [16] lowers the predicted values of M_3 and $d\Delta z/dn$ (not shown). The analytical prediction of the slope $d\Delta z/dn$ using $U_3(r)$ and the

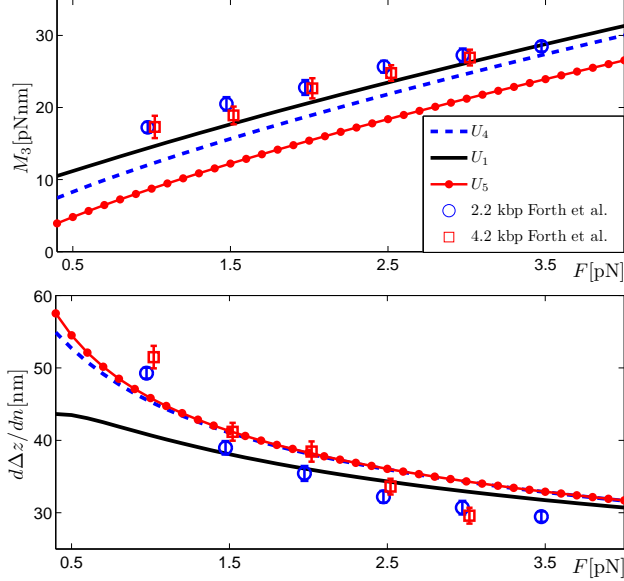


Figure S.2.2: Comparison between the solutions based on different internal energy models under the experimental conditions of Forth et al. [17]. The black solid line uses $U_1 = U_{PB}(r, \theta) + U_{conf}(r, \theta)$, the blue dashed line uses the internal energy model where the radial fluctuations in the plectoneme are constrained by the electrostatics $U_4 = U_{PB}(r, \theta, d_r) + U_{conf}(r, \theta, d_r)$ [12] and the red dotted line uses a model that neglects the configurational entropy contribution to the free energy $U_5 = U_{PB}(r, \theta)$. The qualitative behavior of M_3 and $d\Delta z/dn$ are independent of the internal energy models we have used, but the quantitative agreement with experimental data strongly depends on the choice of configurational entropy model. The value of the effective linear charge used is $\nu=8.06$ [nm^{-1}].

prediction using $U_1(r, \theta)$ are almost identical to each other. It is clear from the graphs that the three approaches produce consistent results for the values of M_3 although the U_2 model gives slightly larger values of M_3 for $F > \sim 2.5 \text{ pN}$. The difference between the U_2 model and the U_1 model at moderate and large F is more evident in the predicted values of $d\Delta z/dn$, where the U_2 model predicts larger slopes. We also performed calculations for different salt concentrations and observed similar trends (not shown).

In Figure S.2.2 we compare the solution obtained by using $U_1(r, \theta)$ with the solution obtained by using the undulation-enhanced free energy model $U_4(r, \theta, d_r)$ with empirically optimized coefficients by van der Maarel[19] $c_p = c_r = 2^{-8/3}$. Figure S.2.2 also depicts the solution obtained by picking $U_5(r, \theta) = U_{PB}(r, \theta)$ with $c_p = c_r = 0$ such that the configurational entropy effects are neglected as done in Clauvelin et al. [11]. It is clear from Figure S.2.2 that the final qualitative behavior of the curves is the same, but the quantitative agreement strongly depends on the choice of the internal energy, in particular, of the configurational entropy model and coefficients. When

comparing U_1 and U_5 we can see that neglecting the entropy effects reduces the internal energy U , increases the value of $d\Delta z/dn$ (mainly at low forces $F < \sim 2pN$) and reduces the predicted value of M_3 (in the whole range of F). The U_5 model neglecting entropy effects used by Clauvelin et al. [11] matches the slope predictions using the U_4 model, but the theoretical results for M_3 using U_5 are lower than the ones predicted using the U_4 model.

Now we are in position to understand how combining different approximations and assumptions can counteract each other. Starting with the U_2 model, if we next neglect the entropic effects as in $U = U_{MS}(r, \theta)$, we get larger slopes at low forces (matching qualitatively better the shape of the experimental trend in Figure S.2.1), but we still overestimate the values of the slopes at larger F . This assumption also decreases the predicted values of M_3 . If we further assume $U = U_{MS}(r)$ where there is no angle dependence, the values of the slopes in the whole F range would decrease giving better quantitative agreement with experimental data of the slopes in Figure S.2.1, and it will decrease the predicted values of M_3 even more. Therefore using the $U_{MS}(r)$ model would 'seem' to accurately match the experimental slopes but it will underestimate the values of M_3 for the whole range of F , especially at low values of $F < \sim 2pN$.

As mentioned in the main text although the data sets for the slopes from different experimental groups and MC simulations agree quantitatively [17, 20–22], this is not the case for the direct and indirect measurements of the torque M_3 . The indirect torque measurements in Mosconi et al. [22] are significantly smaller than the direct measurements taken by Forth et al. [17], Lipfert et al. [23] and the MC simulations in Maffeo et al. [21]. The $U_{MS}(r)$ model combined with a mechanical description in Neukirch and Marko [16] seems to give good agreement with the indirect measurements of the torque M_3 in Mosconi et al. [22], specially at large forces and accurately describe the slope data of the same experimental group. In Maffeo et al. [21] the authors provide also an analytical model that matches the experimental data in Mosconi et al. [22], but does not match the predicted M_3 and r from their MC simulations. In their supplemental material, Maffeo et al. discuss the reasons for the success of their approach as well as its disadvantages and limitations of neglecting fluctuations and entropic terms. They conclude that the reason why their analytical

predictions of M_3 are lower by $\approx 1.5\text{pNnm}$ than their MC simulations is due to neglecting configurational entropy and fluctuation effects. They show that neglecting the entropic effects and undulation enhancement decreases significantly the theoretical predictions of M_3 , while the effects in the theoretical slope predictions is not so drastic. The reason for the drastic increase in the analytical values of M_3 computed in Maffeo et al. [21] when using the entropic model proposed by Ubbink and Odijk [12] lies in the fact that the authors have used $c_p = c_r = 3/2^{8/3}$, which increases the entropic contribution by 3 times compared to the constants used in our $U_{PB}(r, \theta, d_r)$ model in the main text. The constants $c_p = c_r = 3/2^{8/3}$ were derived for a one dimensional worm-like chain confined in a harmonic potential. In the main text we have decided to use the values $c_p = c_r = 2^{-8/3}$ as van der Maarel [19] has suggested.

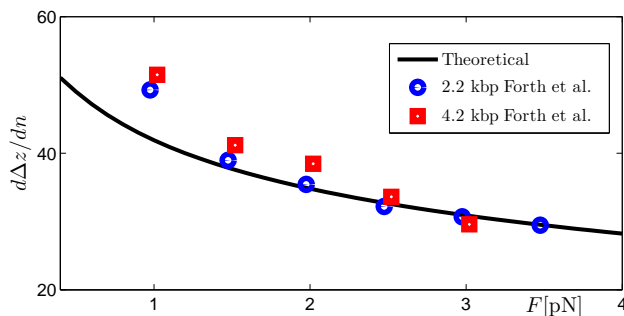


Figure S.2.3: Experimental data for the slope of the rotation-extension curve for two DNA templates taken from Forth et al. [17] for a 150mM salt concentration. We have used $\nu = 5.93\text{nm}^{-1}$.

From Figures S.2.1 and S.2.2 we see that the experimental slopes of Forth et al. [17] are better described qualitatively by using the internal energy model $U_4(r, \theta, d_r)$, and that the theoretical predictions of M_3 using U_4 underestimate the experimental measurements of Forth et al. [17]. Using $\nu < 8.06\text{nm}^{-1}$ in $U_4(r, \theta, d_r)$ gives better quantitative agreement for the slopes, so in the main text we have used the effective linear charge as a fitting parameter. Figure S.2.3 shows the results of $d\Delta z/dn$ from our theoretical model using $\nu = 5.93\text{nm}^{-1}$.

This survey of some of the internal energy models used to study DNA single molecule experiments leads to the conclusion that a careful choice of entropic and electrostatic parameters is needed to quantitatively match the experimental data. We have found that including angle dependence, configurational entropy and undulation enhanced effects due to thermal fluctuations

in the helices are essential to have an accurate and complete model of plectonemic DNA. The $U_4(r, \theta, d_r) = U_{PB} + U_{conf}$ [12] model used in the main text provides the best results for a wide range of experimental data.

S.3 Critical torque $M_{critical}$ and the jump $\delta M = M_{critical} - M_3$

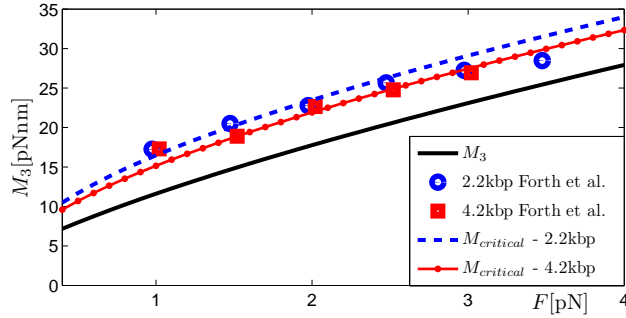


Figure S.3.1: Experimental data for two DNA templates taken from Forth et al. [17] for a 150mM salt concentration. The experimental data of the plectonemic torque in Forth et al. [17] agrees qualitatively with our predictions but seems to match quantitatively our predicted values of $M_{critical}$. We have used $\nu = 5.93\text{nm}^{-1}$.

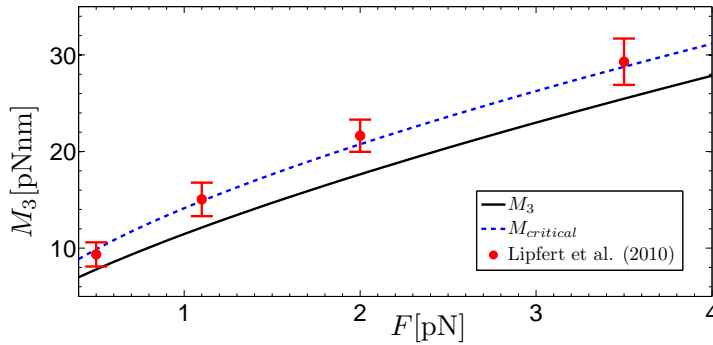


Figure S.3.2: External torque M_3 and critical torque $M_{critical}$ as a function of the external force F for a 7.9 kbp DNA template in a $c_o = 150\text{mM}$ salt concentration using the same parameters as in Figure S.2.3. The data points correspond to the experimental values for the 'buckling' torque reported in Lipfert et al. [23].

The experimental data in Forth et al. [17] shows the jumps in the vertical extension but does not show a clear jump in the torque, and consequently there is no clear distinction between the torque before and after the transition. As shown in Figure S.3.1 the experimental data of the plectonemic torque in Forth et al. [17] agrees qualitatively with our twisting moment predictions M_3 , but seems to match quantitatively our predicted values of the critical torque $M_{critical}$. Lipfert

et al. [23] performed single molecule measurements in PBS buffer at $c_o \approx 150\text{mM}$ using a 7.9 kbp DNA template. The data in Lipfert et al. [23] does not show the transition jumps in either torque or extension. Lipfert et al. [23] just report a ‘buckling torque’ by not making a distinction between the torque before the transition $M_{critical}$ and the plectonemic torque M_3 . Figure S.3.2 shows excellent agreement between our predicted values of $M_{critical}$ and the ‘buckling’ torques in Lipfert et al. [23].

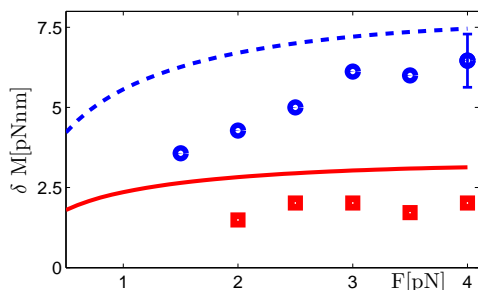


Figure S.3.3: Comparison of the the torque jump δM from our theory with the experiments in Brutzer et al. [20] at $c_o = 320\text{mM}$. Our model predicts that as the DNA length L increase δM decreases while as c_o decreases δM decreases. We have used $\nu = 10.00\text{nm}^{-1}$ as in the main text.

In Figure S.3.3 we show the comparison between δM from the indirect measurements in Brutzer et al. [20] and our theoretical predictions. Similar qualitative trends are found in the indirect measurements of δM in Daniels et al. [7].

S.4 Indirect method for calculating external moment

Mosconi et al. [22] provide not only the direct measurements of the slopes $d\Delta z/dn$ of the rotation-extension curves of a single stretched and twisted DNA molecule using magnetic tweezers, but also an indirect measurement of the plectonemic torque M_3 . The theoretical predictions for the slopes $d\Delta z/dn$ presented in the main text match the experimental results in Mosconi et al. [22], but there seems to be constant 2.5pNnm offset between our theoretical predictions of M_3 and their reported indirect measurements. The process used by Mosconi et al. [22] computes the external

torque M_3 from equation (23) in Zhang and Marko[24]:

$$M_3(F, n) = M_3(F_o, n) - \frac{1}{2\pi} \int_{F_o}^F \left(\frac{\partial \rho L}{\partial n} \right)_{\hat{F}} d\hat{F}, \quad (\text{S.4.1})$$

where F_o is the force corresponding to the initial reference rotation-extension curve. (Eq. (S.4.1)) is based on the ‘Maxwell’ type relation:

$$- \frac{1}{2\pi} \frac{\partial \rho L}{\partial n} \Big|_F = \frac{\partial M_{ext}}{\partial F} \Big|_n. \quad (\text{S.4.2})$$

The method to compute the external torque described in Zhang and Marko [24] assumes the existence of an equilibrium ensemble. So equation (23) in Zhang and Marko [24] is valid in both the straight and plectonemic states. But, at the transition point the system undergoes a dynamic jump from the straight to the plectonemic state or vice-versa. Hence, the method described by Zhang and Marko [24] can not be properly used since the first derivatives of the free energy become discontinuous at the jump. The process carried out to compute the external torques in the plectonemic regime in Mosconi et al. [22] neglects the presence of these jumps. The resolution of the experiments in Mosconi et al. [22] is such that the dynamic process at the transition point between the extended DNA configuration and the plectonemic configuration is not apparent. So, the rotation-extension experimental curves do not show a jump in the extension δz and consequently the external torque curves reported by Mosconi et al. [22] ! show a smooth transition as a function of the degree of supercoiling $\sigma \propto n$. Accounting for the jumps precludes the use of (Eq. (S.4.1)) as done by Mosconi et al. [22].

We note, however, that the method described in Zhang and Marko [24] is valid in the plectonemic regime, as long as there is no dynamic jump. For a set of data containing rotation-extension curves at different values of applied F (for a fixed salt concentration), (Eq. (S.4.1)) can be used to compute a *change* in M_3 by holding n constant and integrating with respect to F . In figure 1 of Mosconi et al. [22] the change in torque M_3 between points A and B can be computed using (Eq. (S.4.1)), but a reference *absolute* value of the torque cannot be obtained using (Eq. (S.4.1))

due to the presence of the jump discontinuity. Since the method described in Zhang and Marko [24] can give the change in M_3 in the plectonemic regime, in Figure S.4.1 we compare our theoretical predictions of the external torque M_3 with the indirect measurements of Mosconi et al. [22] after adding a constant value of 2.5pNnm to the experimental data. The agreement is excellent.

Another possible explanation for the disagreement among the reported theoretical and experimental values of the external moment could be that the values of M_3 in the plectonemic regime are a function of the length of the DNA template, which is a parameter that is not captured in the existent theoretical models including our formulation.

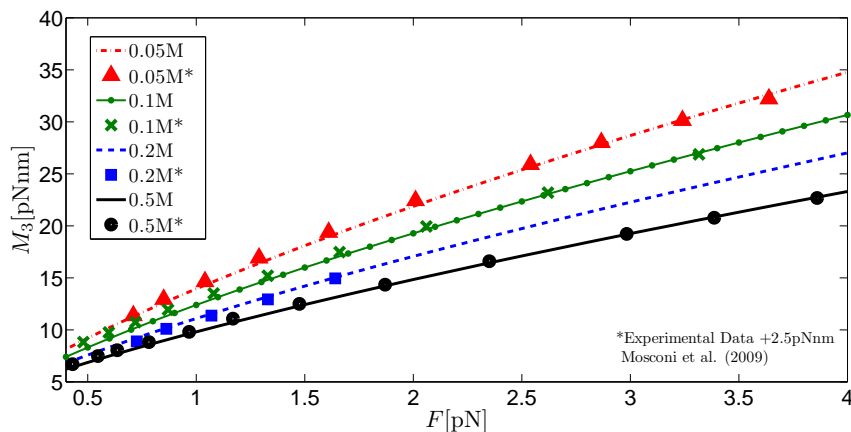


Figure S.4.1: External torque M_3 as a function of the external force F for the different salt concentrations in Mosconi et al. [22]. We show the experimental values from Mosconi et al. [22] after adding a shift of +2.5pNnm. We have used ν values from Table 1 in the main text.

S.5 Multivalent ions

In the main text we have explained how our model can be extended to the case of mixtures of high concentration of monovalent salt and low concentration of polyvalent salt. Here we present further comparison of the theoretical model with the experiments of Dunlap and co-workers (private communication) and show the behavior of the plectoneme radius r and plectonemic torque M_3 as a function of the applied force F . In our calculations we have used ν values from Table 2 in the main text. Figure S.5.1 shows r and M_3 values when using different c_{mu} concentrations

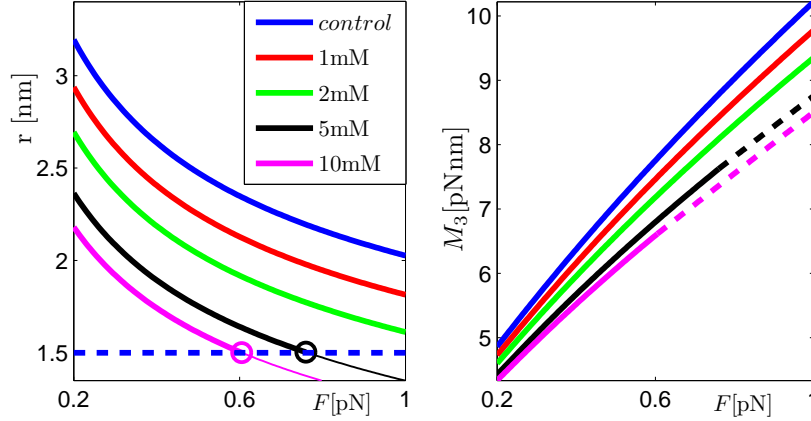


Figure S.5.1: Spermidine: M_3 and r . The dashed lines correspond to the limiting value of the interaxial spacing which is $2r = 3.0\text{nm}$ for spermidine. We have used ν values from Table 2 in the main text.

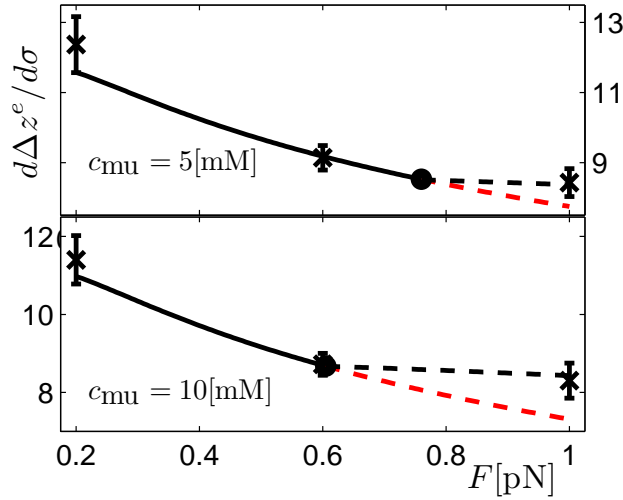


Figure S.5.2: Spermidine: the black solid curve shows the prediction of the slope $d\Delta z^e/d\sigma$ when $2r$ is larger than the interaxial spacing 3nm . The black dot shows the point where $2r = 3\text{nm}$, and from there on the black dashed line shows the prediction of the slope for $2r$ constant. The red dashed line shows the solution when $2r < 3\text{nm}$ is allowed to vary.

of spermidine Sp^{3+} . As c_{mu} increases the supercoiling radius decreases, yielding more compact plectonemes. For $c_{mu} = 5\text{mM}$ and $c_{mu} = 10\text{mM}$ the value of r reaches the limiting interaxial spacing value $\sim 3\text{nm}$ as given in Todd et al.[25] and Raspaud et al.[26]. As explained in the main text we expect that due to a balance of attractive and repulsive interactions the plectoneme diameter stays approximately constant when it reaches the limiting interaxial spacing value. The values of M_3 decrease as a function of c_{mu} . The dashed lines in Figure S.5.1 show M_3 as a function of F for $c_{mu} = 5\text{mM}$ and $c_{mu} = 10\text{mM}$ using $r \approx 1.5\text{nm}$ after the plectoneme diameter has reached the

limiting interaxial spacing value. The theoretical solution of M_3 for $c_{mu} = 5\text{mM}$ and $c_{mu} = 10\text{mM}$ when r is not assumed to be constant does not differ significantly from the solutions plotted in Figure S.5.1. The theoretical solution of the slope $d\Delta z^e/d\sigma$, for $c_{mu} = 5\text{mM}$ and $c_{mu} = 10\text{mM}$, when r is not assumed to be constant differs considerably from the solutions plotted in the main text in Figs. 7 and 8 where r is constant after reaching the interaxial spacing value. If $2r$ is allowed to become smaller than the interaxial distance, the predicted slopes $d\Delta z^e/d\sigma$ underestimate the experimental data at $F = 1\text{pN}$ as shown by the red dashed line in Figure S.5.2.

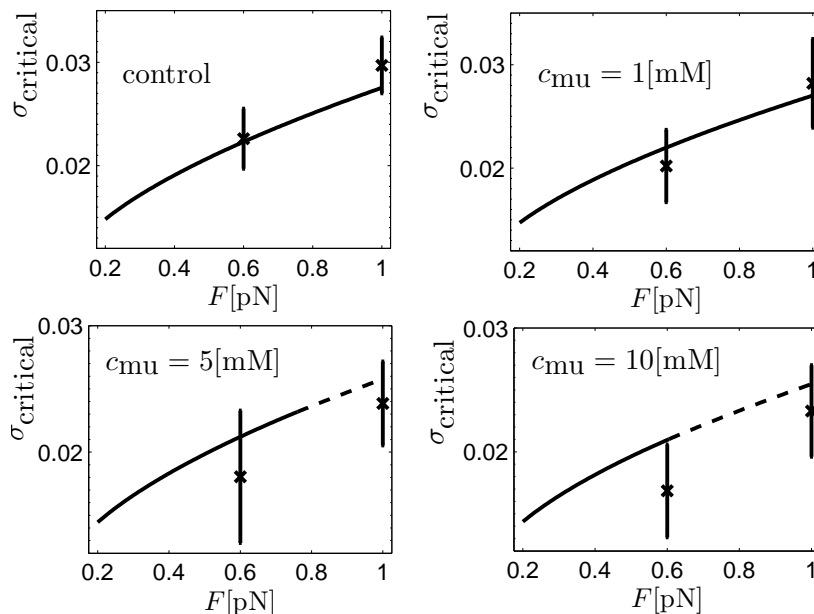


Figure S.5.3: Spermidine: critical degree of supercoiling.

In Figure S.5.3 we present the critical degree of supercoiling $\sigma_{critical} \propto n_{critical}$ when using different c_{mu} concentrations of Sp^{3+} . As stated before the dashed lines in the $c_{mu} = 5\text{mM}$ and $c_{mu} = 10\text{mM}$ cases represent the solution when $2r$ reaches the interaxial spacing value.

Figures S.5.4 and S.5.5 show the results obtained when using spermine Sp^{4+} . For Sp^{4+} we have only fitted the value of ν to the experimental point $F = 0.6\text{pN}$ for the control and $c_{mu} = 0.2 - 0.75\text{mM}$ concentrations and obtained a curve for ν as a function of c_{mu} (see entries in Table 2 in the main text.). For $c_{mu} = 1\text{mM}$ and $c_{mu} = 2\text{mM}$ entries in Table 2 shown in the main text we have extrapolated the value of ν from the curve obtained from the previous fitted values. As before, the dashed lines for the M_3 and $\sigma_{critical}$ function correspond to the solution when $2r$ is approximately

constant and equal to the interaxial spacing $\sim 2.9\text{nm}$ for Sp^{4+} (Todd et al. [25], Raspaud et al. [26]). Our results show good quantitative agreement with the experimental values.

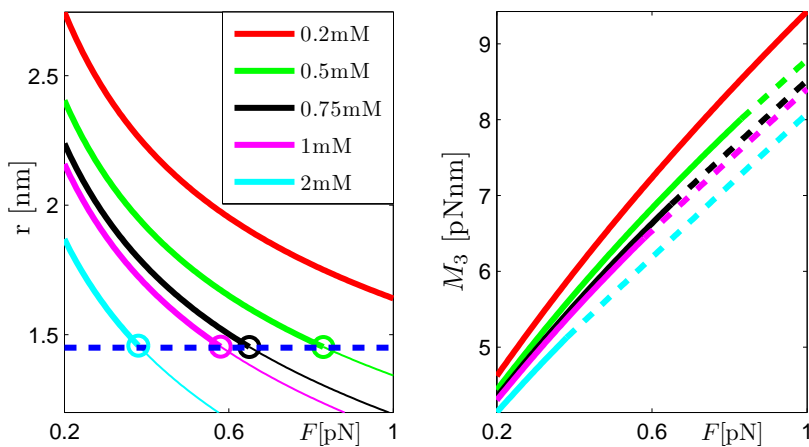


Figure S.5.4: Spermine: M_3 and r . The dashed lines correspond to the limiting value of the interaxial spacing which is $2r = 2.9\text{nm}$ for spermine.

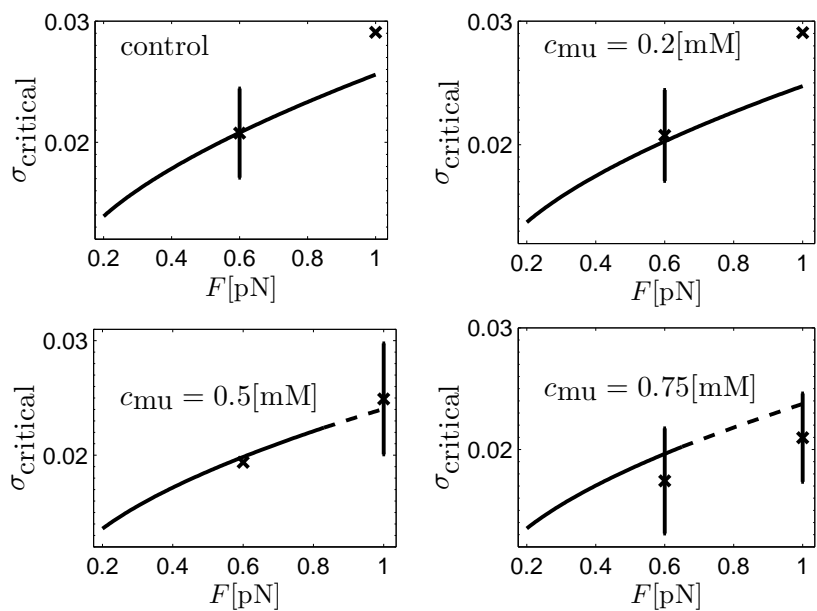


Figure S.5.5: Spermine: critical degree of supercoiling.

S.6 Experimental and Simulation Data

In this section we present the data from all prior experiments and simulations in a few plots so as to compare them independently of our model. A discussion about these plots can be found in the section titled ‘Comparison with experiments and predictions: the complete model’ of the main text.

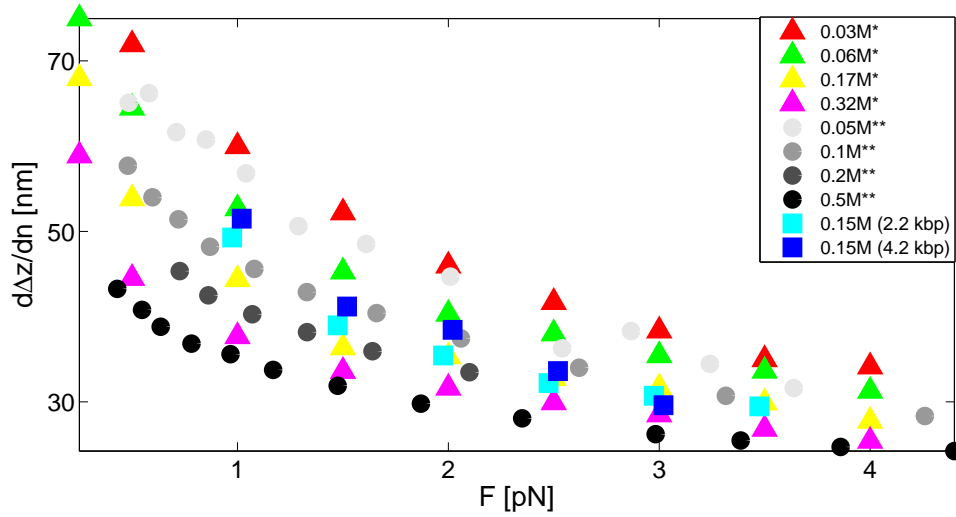


Figure S.6.1: Experimental data for the slopes $d\Delta z/dn$ for different salt concentrations. Triangles represent Brutzer et al. [20] data presented in reference [21]. We have denoted Brutzer et al. data with * next to the salt concentration value in the legend of the graph. Circles represent Mosconi et al. [22] data, which have been denoted with ** next to the salt concentration value in the legend. Squares represent Forth et al. [17] data for two different values of the DNA length. The data sets from Brutzer et al. and Mosconi et al. provide consistent slope values for the entire force range. The slopes from Forth et al.[4] are consistent with the rest of the data sets for moderate forces.

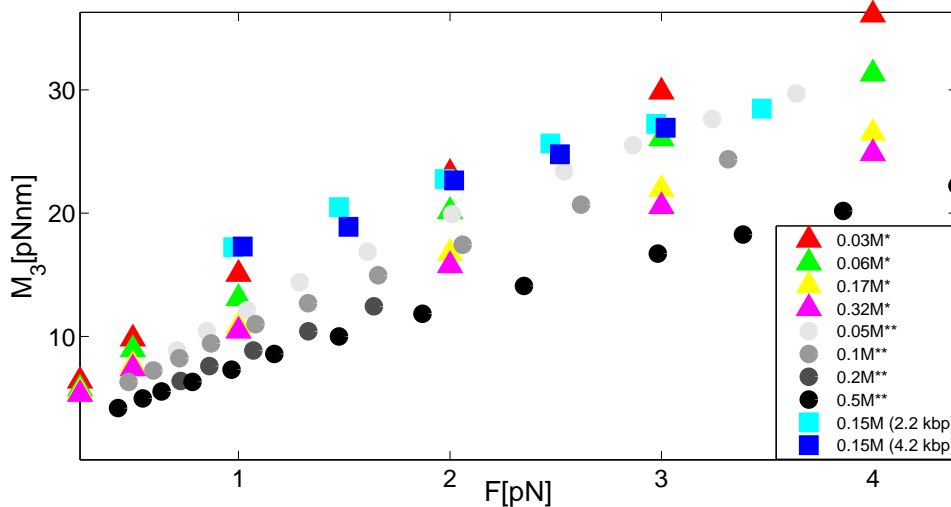


Figure S.6.2: Experimental and Simulations data for the torque measurements M_3 for different salt concentrations. Triangles represent Maffeo et al. [21] simulations data. We have denoted Maffeo et al. data with * next to the salt concentration value in the legend of the graph. Circles represent Mosconi et al. [22] data, which have been denoted with ** next to the salt concentration value in the legend. Squares represent Forth et al. [17] data for two different values of the DNA length. The various data sets show disagreement in the torque values.

References

- (1) Coyne, J. *IEEE J. Oceanic Eng.* **1990**, *15*, 72–83.
- (2) Neukirch, S.; van der Heijden, G.; Thompson, J. *J. Mech. Phys. Solids* **2002**, *50*(6), 1175–1191.
- (3) van der Heijden, G.; Thompson, J. *Nonlinear Dynam.* **2000**, *79*(1), 71–99.
- (4) van der Heijden, G.; Neukirch, S.; Thompson, J. *Int. J. Mech. Sci.* **2003**, *45*(1), 161–196.
- (5) Coleman, B.; Swigon, D. *J. Elasticity* **2000**, *60*, 173 – 221.
- (6) Coleman, B.; Swigon, D. *Nuovi progressi nella fisica matematica dall’eredità di Dario Graffi* **2002**, *177*, 281–295.
- (7) Daniels, B.; Forth, S.; Sheinin, M. Y.; Wang, D.; Sethna, J. P. *Phys. Rev. E.* **2009**, *80*, 040901(R).
- (8) Strick, T.; Allemand, J.; Croquette, V.; Bensimon, D. *Prog. Biophys. Mol. Biol.* **2000**, *74*(1-2), 115–140.

- (9) Kúlic, I. M.; Mohrbach, H.; Thaokar, R.; Schiessel, H. *Phys. Rev. E* **2007**, *75*(1), 011913.
- (10) Agrawal, N. J.; Radhakrishnan, R.; Purohit, P. *Biophys. J.* **2008**, *94*, 3150–3158.
- (11) Clauvelin, N.; Audoly, B.; Neukirch, S. *Biophys. J.* **2009**, *96*(9), 3716–3723.
- (12) Ubbink, J.; Odijk, T. *Biophys. J.* **1999**, *76*(5), 2502–2519.
- (13) Manning, G. *J. Chem. Phys.* **1969**, *51*(3), 954.
- (14) Marko, J.; Siggia, E. *Phys. Rev. E* **1995**, *52*(3), 2912–2938.
- (15) Purohit, P. K. Shape and Energetics of DNA Plectonemes. Chapter in IUTAM book series: "IUTAM Symposium on Cellular, Molecular and Tissue Mechanics", 2010; ISBN 978-90-481-3347-5.
- (16) Neukirch, S.; Marko, J. *Phys. Rev. Lett.* **2011**, *106*(13), 138104.
- (17) Forth, S.; Deufel, C.; Sheinin, M. Y.; Daniels, B.; Sethna, J. P.; Wang, D. *Phys. Rev. Lett.* **2008**, *100*(14), 148301.
- (18) Clauvelin, N.; Audoly, B.; Neukirch, S. *Macromolecules* **2008**, *41*(12), 4479–4483.
- (19) van der Maarel, J. R. C. *Introduction to Biopolymer Physics*; World Scientific: Singapore, 2008.
- (20) Brutzer, H.; Luzziatti, N.; Klaue, D.; Seidel, R. *Biophys. J.* **2010**, *98*(7), 1267–1276.
- (21) Maffeo, C.; Robert, S.; Brutzer, H.; René, S.; Aleksei, A.; Gero, W.; Seidel, R. *Phys. Rev. Lett.* **2010**, *105*(15), 158101.
- (22) Mosconi, F.; Allemand, J.; Bensimon, D.; Croquette, V. *Physical Review Letter* **2009**, *102*(7), 078301.
- (23) Lipfert, J.; Kerssenmakers, J.; Jager, T.; Dekker, N. *Nature Methods* **2010**, published online doi:10.1038/nmeth.1520, (17 October 2010).

(24) Zhang, H.; Marko, J. *Phys. Rev. E* **2008**, *77*(3 Pt 1), 031916.

(25) Todd, B.; Parsegian, V.; Shirahata, A.; Thomas, T.; Rau, D. *Biophys. J.* **2008**, *95*, 4775–4782.

(26) Raspaud, E.; Durand, D.; Livolant, F. *Biophys. J.* **2005**, *88*, 392–403.